Pion absorption from the lowest atomic orbital in ^{2}H, ^{3}H, and ^{3}He

J. Golak, V. Urbanevych, R. Skibiński, H. Witała, and K. Topolnicki
M. Smoluchowski Institute of Physics, Jagiellonian University, PL-30348 Kraków, Poland

V. Baru, A. A. Filin, and E. Epelbaum
Ruhr-Universität Bochum, Fakultät für Physik und Astronomie, Institut für Theoretische Physik II, D-44780 Bochum, Germany

H. Kamada
Department of Physics, Faculty of Engineering, Kyushu Institute of Technology, Kitakyushu 804-8550, Japan

A. Nogga
Institut für Kernphysik (IKP-3), Institute for Advanced Simulation (IAS-4), Center for Advanced Simulation and Analytics (CASA), and Jülich Center for Hadron Physics (JCHP), Forschungszentrum Jülich, D-52425 Jülich, Germany

(Received 7 September 2022; accepted 15 November 2022; published 19 December 2022)

The $\pi^- + {}^2\mathrm{H} \to n + n$, $\pi^- + {}^3\mathrm{H} \to n + n + n$, $\pi^- + {}^3\mathrm{He} \to n + d$, and $\pi^- + {}^3\mathrm{He} \to p + n + n$ capture reactions from the lowest $1S$ atomic orbitals are studied under full inclusion of final state interactions. Our results are obtained with the single-nucleon and two-nucleon transition operators derived at leading order in chiral effective field theory. The initial and final three-nucleon states are calculated with the chiral nucleon-nucleon semilocal momentum space potential up to $\mathrm{N^4LO^+}$, augmented by the consistently regularized chiral $\mathrm{N^2LO}$ three-nucleon potential. We found that absorption rates depend strongly on the nuclear pion absorption operator used, and its two-body parts change the rates by a few orders of magnitude. The final state interactions between nucleons generated by the two-nucleon forces are also important, while the three-nucleon interaction plays a visible role only in the $\pi^- + {}^3\mathrm{He} \to n + d$ reaction. Our absorption rate for the $\pi^- + {}^2\mathrm{H} \to n + n$ process is in good agreement with the experimental data from the hadronic ground-state broadening in pionic deuterium. The capture rates on ^{3}He are also generally consistent with the spectroscopic data within error bars, though our central values are found to be systematically below the data. We show that for the three-body breakup processes the dominant contributions to the absorption rates arise from the quasi-free scattering and final-state interaction kinematical configurations.

DOI: 10.1103/PhysRevC.106.064003

I. INTRODUCTION

Pion production in nucleon-nucleon collisions and the related pion absorption reactions involving nuclei have been extensively studied both experimentally and theoretically. In the mid 1960s intense proton beams of energies between 500 MeV and 1 GeV became available, which led to the construction of the so-called "meson factories": TRIUMF (Canada), SIN (Switzerland), LAMPF (USA), and later also one in the Soviet Union. Consequently, pions were used for a variety of nuclear and particle physics experiments. Absorption reactions are accompanied by scattering processes and the theoretical approaches to these reactions in the 1980s were either based on perturbation theory [1–3] or applied few-body models [4–13]. The latter allowed the authors to satisfy two- and three-body unitarity. That was achieved for the first time by Mizutani and collaborators, who published a series of publications [4–8,11,13] focusing on the coupled-channel πNN-NN systems but also connected kernel equations for the coupled-channel πNNN-NNN systems [14,15]. Experimental and theoretical research conducted by many groups was summarized in several review papers (see for example Refs. [16,17]) and in books, including Refs. [18–21]. The main message of those publications was the dominance of two-nucleon mechanisms for stopped and in-flight pion absorption.

In the early 1990s, the precise experimental data for the total cross section of neutral pion production in proton-proton collisions in the threshold kinematics measured at the Indiana University Cyclotron Facility (IUCF) [22] revealed a serious disagreement with the theoretical calculations by almost an order of magnitude [23,24]. While it was quickly realized that the production mechanism involving the Weinberg-Tomozawa vertex should play an important role for charged pion production [24], this phenomenological model still failed to describe the data by a factor of 2. Various phenomenological attempts to account for the missing physics were made including the heavy meson exchanges, the off-shell πN effects, excitations of baryon resonances, etc.; see Ref. [25] for a review and references therein. These unexpected findings also stimulated extensive theoretical research in the framework of chiral effective field theory (EFT); see [26] for a review.

The studies of the $NN \to NN\pi$ reactions have revealed a number of interesting aspects. The first tree-level EFT calculations, carried out up to next-to-next-to leading order (N^2LO) in the original Weinberg counting [27], did not actually show any significant improvements [28–32]. Moreover, the N^2LO corrections at one-loop order [33,34] were found to be even larger than the NLO ones, calling the convergence of the Weinberg EFT into question [35]. On the other hand, researchers soon realized the important role played by the momentum scale $p \sim \sqrt{M_\pi M}$ associated with real pion production [28,31,36,37]. Here, M_π and M refer to the pion and nucleon masses, respectively. In particular, the order-of-magnitude differences between various one-loop diagrams of Ref. [33] could be naturally understood if this new scale is included in the power counting [25]. Thus, the appearance of this scale requires the appropriate modification of the chiral power counting as compared to the standard framework used to describe few-nucleon reactions below pion-production threshold; see Refs. [38–40] for review articles. The use of this new counting scheme, now known as the momentum counting scheme (MCS), led to a very good understanding of the threshold charge pion production data already at leading order in the MCS (LO-MCS) [41]. Later on, the calculation was pushed forward to the N^2LO-MCS [42–44].

Another interesting aspect of P-wave pion production in NN collisions is the fact that the leading short-range mechanism is the same as the one in the dominant three-nucleon force [45], the axial-vector current operator [46–49], as well as in the reactions $\gamma\ ^2\mathrm{H} \to \pi NN$ [50,51] and $\pi\ ^2\mathrm{H} \to \gamma NN$ [48]. Thus, the reaction $NN \to NN\pi$ can, at least in principle, be used to determine the corresponding low-energy constant c_D and to test consistency of chiral EFT. More recently, pion production in two-nucleon collisions gained considerable interest in connection with charge-symmetry breaking. Specifically, the experimental measurement of the charge-symmetry breaking forward-backward asymmetry in the $pn \to d\pi^0$ reaction [52] has been argued to provide access to the strong-interaction proton-neutron mass difference [53]. This quantity was extracted in Ref. [54] based on the $A_{fb}(pn \to d\pi^0)$ data; see also Ref. [55] for a related study. The cross section in the reaction $dd \to {}^4\mathrm{He}\,\pi^0$ measured at IUCF and later also by the WASA-at-COSY Collaboration [56,57] is yet another very clean probe of charge symmetry breaking, but it still lacks a reliable theoretical analysis due to the required complicated treatment of the four-nucleon continuum; see, however, [58] for a first step along this line.

Experimental data for near-threshold pion production in nucleon-deuteron collisions are also available—see, e.g., [59–61] as well as spectroscopic data on $\pi\ ^3\mathrm{He}$ atoms [62–65]—but theoretical efforts are very scarce as compared with the two-nucleon sector; see, e.g., [66,67]. In particular, we are not aware of any calculations in the framework of chiral EFT.

In this paper we focus on the inverse of the pion production processes mentioned above. Specifically, we perform an exploratory study of stopped π^- absorption out of the lowest orbitals of $^2\mathrm{H}$, $^3\mathrm{H}$, and $^3\mathrm{He}$ pionic atoms. Pion absorption is an important subprocess for the pion scattering reactions that gained a considerable interest in connection with the determination of the corresponding scattering lengths. It does not only govern the imaginary part of the scattering length, but also contributes to its real part via the so-called dispersive corrections. Chiral EFT calculations of the pion-deuteron scattering length and the extraction of the pion-nucleon scattering lengths can be found in Refs. [68–70]. For related studies of pion production in proton-proton collisions and the π-^{3}He and π-^{4}He scattering lengths see Refs. [71,72].

Results presented here are obtained within the formalism of the Faddeev equations, which is one of standard approaches in three-nucleon studies. It was first applied to three-nucleon bound states (3NBS) and nucleon-deuteron scattering; see [73] and references therein. Over time, this formalism has been extended to other processes, such as electron-3NBS scattering [74] and 3NBS photodisintegration [75] and further to various electroweak processes including muon capture [76–79], neutrino scattering [80,81], and pion radiative capture [82]. An important advantage of this formalism is its flexibility. It enables us to use various models of nuclear forces or currents, and to easily identify effects of various dynamical ingredients, such as final state interactions or three-nucleon forces.

The paper is organized in the following way. In Sec. II we introduce the single-nucleon and two-nucleon pion absorption operators, which we treat in momentum space. In the following section we show results for the $\pi^- + {}^2\mathrm{H} \to n + n$ and $\pi^- + {}^3\mathrm{He} \to n + d$ two-body reactions. Our results for the three-body processes, $\pi^- + {}^3\mathrm{He} \to p + n + n$ and $\pi^- + {}^3\mathrm{H} \to n + n + n$, are shown in Sec. IV, where we discuss in detail the way we calculate the total absorption rates and present various predictions for the differential absorption rates calculated with different three-nucleon dynamics. In these calculations we employ the chiral semilocal momentum space (SMS) nucleon-nucleon potentials up to N^4LO^+ [83] and the N^2LO three-nucleon forces [84]. Finally, Sec. V contains some concluding remarks.

II. THE TRANSITION OPERATOR

In the negative pion absorption process we assume that the initial state $|i\rangle$ consists of the atomic K-shell pion wave function $|\phi\rangle$ and the initial nucleus state with the three-momentum $\mathbf{P}_i$ and the spin projection m_i:

$$|i\rangle = |\phi\rangle|\Psi_i\,\mathbf{P}_i\,m_i\rangle. \tag{2.1}$$

The final state, $|f\rangle$, is the nuclear state with the total three-momentum $\mathbf{P}_f$ and the set of spin projections m_f:

$$|f\rangle = |\Psi_f\,\mathbf{P}_f\,m_f\rangle. \tag{2.2}$$

The transition from the initial to final state is given in terms of the nuclear matrix element N of the nuclear transition operator ρ between the initial and final nuclear states:

$$N = \langle\Psi_f\,\mathbf{P}_f\,m_f|\rho|\Psi_i\,\mathbf{P}_i\,m_i\rangle. \tag{2.3}$$

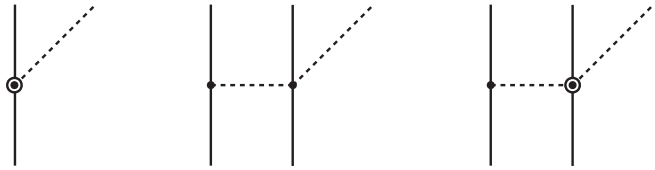

FIG. 1. Diagrams contributing to the pion production operator at LO in the MCS. Solid and dashed lines denote nucleons and pions, respectively. Solid dots are the pion-nucleon vertices from the lowest-order effective chiral Lagrangian, while circled dots denote the corresponding relativistic $1/M$ corrections.

The ρ operator contains single-nucleon (SN), two-nucleon (2N) and, in principle also many-nucleon [such as three-nucleon (3N)] contributions but in the present paper we restrict ourselves to the SN and 2N parts. We use the fact that the 3N operators are suppressed compared to the SN and 2N ones by the power counting.

As already pointed out in the Introduction, the pion production operator has been extensively studied within the so-called momentum counting scheme (MCS), which is an extension of the standard chiral EFT power counting to account for the momentum scale $p \sim \sqrt{M_\pi M}$. In particular, the leading-order (LO-MCS) contribution has been worked out in Ref. [41]. The corrections up to next-to-next-to-leading order in the MCS have been derived in Refs. [42,43] including the explicit contributions of the $\Delta(1232)$ resonance and implemented in Ref. [44], see also Ref. [26] for a review. These corrections have been implemented in Ref. [44] to study the cross section of the reaction $p + p \to {}^2\mathrm{H} + \pi^+$ in the threshold kinematics. While the results of Refs. [41,44] showed good agreement with data, they were obtained using modern phenomenological NN potentials only. On the other hand, it was argued in Ref. [44] that the chiral interactions available at that time, regularized in a coordinate-space, were generated with a cutoff, which tends to remove a part of the intermediate-range physics relevant for pion production in NN collisions.

In this exploratory study, we would like to update the previous analysis by using the modern SMS chiral NN potentials [83], which are softer than the coordinate-space regularized potentials and therefore expected to be more suitable for studying the pion production process. Furthermore, we will use the calculation of the $\pi^- + {}^2\mathrm{H} \to n + n$ channel, which is directly related to $p + p \to {}^2\mathrm{H} + \pi^+$ via detailed balance, as benchmark to present the first EFT-based predictions for the pion absorption rate on ^{3}He and ^{3}H. For these purposes, we limit ourselves to the LO-MCS contributions to the transition operator, which emerge from the direct diagram (a) and the two rescattering graphs (b) and (c) as shown in Fig. 1. Notice that the static LO pion-nucleon vertex proportional to the nucleon axial vector coupling g_A does not contribute to the direct term of type (a) due to the threshold kinematics. We further emphasize that, in addition to the rescattering diagram (b) with the Weinberg-Tomozawa (WT) $\pi\pi NN$ vertex, one also has to take into account diagram (c), which involves a $1/M$ correction to the WT vertex. The appearance of both graphs at LO is the well-known peculiar feature of the kinematics involved in the pion production reaction. The explicit expressions for the SN (direct) and 2N parts of the production operator are well known and will be specified below. Notice further that we do not employ any regulator for the 2N transition operator in this study. We also stress that even though some of the numerical results discussed below are based on the nuclear forces and the pion production operator derived in chiral EFT, our approach is to be regarded as a hybrid one. This is because the employed nuclear potentials are derived assuming the kinematics with the nucleon momenta of the order of $\sim M_\pi$, and they should be applied, strictly speaking, only below the pion production threshold.

The momentum-space matrix element of the SN pion absorption operator $\rho(1)$ [85], for nucleon 1, which depends on the nucleon incoming ($\mathbf{p}$) and outgoing ($\mathbf{p}'$) momentum, is given by

$$\langle \mathbf{p}'|\rho(1)|\mathbf{p}\rangle = -\frac{g_A M_\pi}{\sqrt{2}F_\pi}\,\frac{(\mathbf{p}'+\mathbf{p})\cdot\boldsymbol{\sigma}_1}{2M}\,(\boldsymbol{\tau}_1)_-, \qquad (2.4)$$

where $g_A = 1.29$, $F_\pi = 92.4$ MeV, and $M_\pi = 139.57$ MeV refer to the nucleon axial vector coupling, pion decay constant, and negative pion mass, respectively. $\rho(1)$ is still an operator in the spin and isospin spaces, with $\boldsymbol{\sigma}_1$ ($\boldsymbol{\tau}_1$) being the Pauli spin (isospin) operator for nucleon 1 and the isospin lowering operator $(\boldsymbol{\tau}_1)_- \equiv [(\boldsymbol{\tau}_1)_x - \mathrm{i}(\boldsymbol{\tau}_1)_y]/2$. The effects stemming from the small difference between the proton mass M_p and neutron mass M_n are beyond the accuracy level of our LO absorption operator and we use the average "nucleon mass," $M \equiv \frac{1}{2}(M_p + M_n)$.

We represent 2N and 3N states using partial wave decomposition and remind the reader of its basic ingredients. The 2N momentum space partial wave states, $|p\alpha_2\rangle \equiv |p(ls)jm_j;tm_t\rangle$, carry information about the magnitude of the relative momentum (p), the relative angular momentum (l), spin (s), and total angular momentum (j) with the corresponding projection (m_j). This set of quantum numbers is augmented by the 2N isospin (t) and its projection (m_t).

The corresponding "(2, 3)1" 3N states $|pq\alpha\rangle \equiv |p(ls)\,j\,q(\lambda\tfrac{1}{2})I\,(jI)Jm_J;Tm_T\rangle$ are built on top of the subsystem (2,3) quantum numbers and contain additionally information about nucleon 1: the magnitude of its relative momentum with respect to the center of mass (c.m.) of the (2,3) subsystem (q), relative orbital angular momentum (λ), total spin of nucleon 1 (I), and, finally, the total 3N angular momentum (J) with the projection (m_J) resulting from coupling of the 2-3 subsystem j and spectator I angular momenta. The total 3N isospin state, $|(t\tfrac{1}{2})Tm_T\rangle$ is included analogously [74]. Note that such full 3N partial-wave states are already antisymmetrized in the (2,3) subsystem.

In the case of the single-nucleon pion absorption operator applied to the initial deuteron state with the spin

projection m_d and total momentum $\mathbf{P}_i$, we can use a general formula [76]

$$\begin{aligned}\langle p(ls)jm_j\,;tm_t\,\mathbf{P}_f|\rho(1)|\phi_d\,m_d\,\mathbf{P}_i\rangle =\ & \delta_{t,1}\,\delta_{m_t,-1}\,\langle 1\ -1|(\boldsymbol{\tau}_1)_-|00\rangle\sum_{m_l} c(l,s,j;m_l,m_j-m_l,m_j)\\ &\times\sum_{l_d=0,2}\sum_{m_{l_d}} c(l_d,1,1;m_{l_d},m_d-m_{l_d},m_d)\sum_{m_1} c\left(\frac{1}{2},\frac{1}{2},s;m_1,m_j-m_l-m_1,m_j-m_l\right)\\ &\times\sum_{\mu_1} c\left(\frac{1}{2},\frac{1}{2},1;\mu_1,m_d-m_{l_d}-\mu_1,m_d-m_{l_d}\right)\\ &\times\ \delta_{m_j-m_l-m_1,m_d-m_{l_d}-\mu_1}\int d\hat{\mathbf{p}}\,Y^*_{l\,m_l}(\hat{\mathbf{p}})\,Y_{l_d\,m_{l_d}}\left(\widehat{\mathbf{p}-\frac{1}{2}\mathbf{Q}}\right)\varphi_{l_d}\left(\left|\mathbf{p}-\frac{1}{2}\mathbf{Q}\right|\right)\\ &\times\left\langle\frac{1}{2}m_1\middle|\left\langle\mathbf{p}+\frac{1}{2}\mathbf{P}_f\middle|\rho(1)\middle|\mathbf{p}-\frac{1}{2}\mathbf{P}_f+\mathbf{P}_i\right\rangle\middle|\frac{1}{2}\mu_1\right\rangle,\end{aligned}\tag{2.5}$$

where $\mathbf{Q}\equiv\mathbf{P}_f-\mathbf{P}_i$, $c(j_1,j_2,j;m_1,m_2,m)$ are Clebsch-Gordan coefficients and the internal deuteron state contains two components,

$$|\phi_d\,m_d\rangle=\sum_{l_d=0,2}\int dp\,p^2|p(l_d1)1m_d\,;00\rangle\varphi_{l_d}(p).\tag{2.6}$$

We could in principle utilize the so-called automatized partial wave decomposition method [86,87]: prepare momentum dependent spin matrix elements

$$\left\langle\tfrac{1}{2}m'\middle|\langle\mathbf{p}_1{}'|\rho(1)|\mathbf{p}_1\rangle\middle|\tfrac{1}{2}m\right\rangle\tag{2.7}$$

and compute the double integral over

$$\int d\hat{\mathbf{p}}\equiv\int_0^{2\pi}d\phi_p\int_0^{\pi}d\theta_p\sin\theta_p\tag{2.8}$$

numerically. However, for the absorption of a stopped pion on a nuclear system at rest we can assume here and in the following that $\mathbf{P}_i=\mathbf{P}_f=0$ and benefit from the simple form of $\rho(1)$, which leads to the conservation of the 2N total angular momentum and to the change of the 2N parity. As a result, matrix elements (2.5) are nonzero for just *one* partial wave state with $l=1$, $s=1$, $j=1$, and $m_j=m_d$:

$$\begin{aligned}&\langle p(11)1m_j;1\ -1\,\mathbf{P}_f=0|\rho(1)|\phi_d\,m_d\,\mathbf{P}_i=0\rangle\\ &\quad=\delta_{m_j,m_d}\frac{g_AM_\pi}{2\sqrt{2}MF_\pi}\,p\,\frac{2\varphi_0(p)+\sqrt{2}\varphi_2(p)}{\sqrt{3}}.\end{aligned}\tag{2.9}$$

A general formula is also easy to obtain for a SN operator applied to a 3N bound state $|\Psi\,m_b\,;\frac{1}{2}m_{T_b}\,\mathbf{P}_i\rangle$ with the spin $J_b=\frac{1}{2}$, spin projection m_b, isospin $T_b=\frac{1}{2}$, isospin projection m_{T_b}, and the total momentum $\mathbf{P}_i$, represented in the 3N partial wave states α_b:

$$\begin{aligned}\langle pq\alpha\,\mathbf{P}_f|\rho(1)|\Psi\,m_b\,;\frac{1}{2}m_{T_b}\,\mathbf{P}_i\rangle =\ & \sum_{\alpha_b}\delta_{l,l_b}\,\delta_{s,s_b}\,\delta_{j,j_b}\,\delta_{t,t_b}\,\delta_{m_T,m_{T_b}-1}\left\langle\left(t\,\frac{1}{2}\right)T\ m_T\middle|(\boldsymbol{\tau}_1)_-\middle|\left(t_b\frac{1}{2}\right)\frac{1}{2}\ m_{T_b}\right\rangle\\ &\times\sum_{m_j}c(j,I,J;m_j,m_J-m_j,m_J)\,c\left(j_b,I_b,\frac{1}{2};m_j,m_b-m_j,m_b\right)\\ &\times\sum_{m_\lambda}c\left(\lambda,\frac{1}{2},I;m_\lambda,m_J-m_j-m_\lambda,m_J-m_j\right)\\ &\times\sum_{m_{\lambda_b}}c\left(\lambda_b,\frac{1}{2},I_b;m_{\lambda_b},m_b-m_j-m_{\lambda_b},m_b-m_j\right)\\ &\times\int d\hat{\mathbf{q}}\,Y^*_{\lambda\,m_\lambda}(\hat{\mathbf{q}})\,Y_{\lambda_b\,m_{\lambda_b}}\left(\widehat{\mathbf{q}-\frac{2}{3}\mathbf{Q}}\right)\phi_{\alpha_b}\left(p,\left|\mathbf{q}-\frac{2}{3}\mathbf{Q}\right|\right)\\ &\times\left\langle\frac{1}{2}\,m_J-m_j-m_\lambda\middle|\left\langle\mathbf{q}+\frac{1}{3}\mathbf{P}_f\middle|\rho(1)\middle|\mathbf{q}-\frac{2}{3}\mathbf{P}_f+\mathbf{P}_i\right\rangle\middle|\frac{1}{2}\,m_b-m_j-m_{\lambda_b}\right\rangle\end{aligned}\tag{2.10}$$

where, as in the 2N space, $\mathbf{Q}\equiv\mathbf{P}_f-\mathbf{P}_i$. The initial 3N bound state is given as

$$\left|\Psi\,m_b\,;\frac{1}{2}m_{T_b}\right\rangle=\sum_{\alpha_b}\int dpp^2\int dqq^2\,|pq\alpha_b\rangle\phi_{\alpha_b}(p,q).\tag{2.11}$$

For $\rho(1)$ the result given in Eq. (2.10) can be simplified, especially for $\mathbf{P}_i = \mathbf{P}_f = 0$, and written as

$$\begin{aligned}\left\langle pq\alpha\, \mathbf{P}_f = 0|\rho(1)\right|\Psi\, m_b\,; \frac{1}{2} m_{T_b}\, \mathbf{P}_i = 0\Big\rangle &= \frac{g_A M_\pi \sqrt{6}}{M F_\pi}\, q\, \delta_{m_T, m_{T_b}-1}\, \delta_{J,\frac{1}{2}}\, \delta_{m_J, m_b} \sqrt{(2\lambda+1)}\, (-1)^{I+\frac{1}{2}} \\ &\times (-1)^t \begin{Bmatrix} 1 & \frac{1}{2} & \frac{1}{2} \\ t & T & \frac{1}{2} \end{Bmatrix} c\left(1, \frac{1}{2}, T; -1, m_{T_b}, m_{T_b}-1\right) \\ &\times \sum_{\alpha_b} \delta_{l,l_b}\, \delta_{s,s_b}\, \delta_{j,j_b}\, \delta_{t,t_b}\, \delta_{I,I_b}\, \phi_{\alpha_b}(p,q) \\ &\times \sqrt{(2\lambda_b+1)}\, c(\lambda, \lambda_b, 1; 0, 0, 0) \begin{Bmatrix} \lambda & \lambda_b & 1 \\ \frac{1}{2} & \frac{1}{2} & I \end{Bmatrix}, \end{aligned} \tag{2.12}$$

where the change of the 3N parity follows from the property of the Clebsch-Gordan coefficient $c(\lambda, \lambda_b, 1; 0, 0, 0)$, which is nonzero only for odd $\lambda + \lambda_b$.

The 2N part of ρ at LO, stemming from the rescattering diagrams (b) and (c) of Fig. 1, has the form [41]

$$\langle \mathbf{p}_1' \mathbf{p}_2' | \rho(1,2) | \mathbf{p}_1 \mathbf{p}_2 \rangle = (v(k_2)\mathbf{k}_2 \cdot \boldsymbol{\sigma}_2 - v(k_1)\mathbf{k}_1 \cdot \boldsymbol{\sigma}_1) \frac{i}{\sqrt{2}} [(\boldsymbol{\tau}_1 \times \boldsymbol{\tau}_2)_x - i(\boldsymbol{\tau}_1 \times \boldsymbol{\tau}_2)_y], \tag{2.13}$$

where $\mathbf{k}_1 = \mathbf{p}_1' - \mathbf{p}_1$, $\mathbf{k}_2 = \mathbf{p}_2' - \mathbf{p}_2$ and the form factor $v(k)$ reads

$$v(k) = \frac{1}{(2\pi)^3} \frac{g_A M_\pi}{4F_\pi^3} \frac{1}{M_\pi^2 + k^2}. \tag{2.14}$$

For the operator defined in (2.13) it is sufficient to calculate the corresponding matrix elements without isospin,

$$H(p', \bar{\alpha}_2'; p, \bar{\alpha}_2) \equiv \langle p'(l's')j'm_{j'} | \rho(1,2)^{\text{spin}} | p(ls)jm_j \rangle, \tag{2.15}$$

where

$$\langle \mathbf{p}_1' \mathbf{p}_2' | \rho(1,2)^{\text{spin}} | \mathbf{p}_1 \mathbf{p}_2 \rangle = v(k_2)\mathbf{k}_2 \cdot \boldsymbol{\sigma}_2 - v(k_1)\mathbf{k}_1 \cdot \boldsymbol{\sigma}_1, \tag{2.16}$$

and supplement them later with appropriate 2N or 3N isospin matrix elements [74]. For $\mathbf{P}_i = \mathbf{P}_f = 0$ one gets simply

$$v(k_2)\mathbf{k}_2 \cdot \boldsymbol{\sigma}_2 - v(k_1)\mathbf{k}_1 \cdot \boldsymbol{\sigma}_1 = -v(k_1)\mathbf{k}_1 \cdot (\boldsymbol{\sigma}_1 + \boldsymbol{\sigma}_2) \tag{2.17}$$

and the $\mathbf{k}_1$ vector is just the difference between the final and initial relative momenta, $\mathbf{k}_1 = \mathbf{p}' - \mathbf{p}$. Equation (2.17) constitutes a convenient starting point for analytical evaluation of $H(p', \bar{\alpha}_2'; p, \bar{\alpha}_2)$. Standard steps [88] using multiple recouplings of angular momenta, properties of the spherical harmonics, and Clebsch-Gordan coefficients lead to

$$\begin{aligned}\langle p'(l's')j'm_{j'} | \rho(2,3)^{\text{spin}} | p(ls)jm_j \rangle &= \delta_{j,j'}\, \delta_{m_j, m_{j'}}\, \delta_{s,1}\, \delta_{s',1}\, 12\pi\sqrt{2}\, (-1)^j \begin{Bmatrix} l & l' & 1 \\ 1 & 1 & j \end{Bmatrix} \\ &\times \sum_{a_1+a_2=1} (p')^{a_1}\, p^{a_2}\, (-1)^{a_2} \sum_w (2w+1)\, (-1)^w\, g_w(p', p) \\ &\times \begin{Bmatrix} l & l' & 1 \\ a_1 & a_2 & w \end{Bmatrix} c(w, a_1, l'; 0, 0, 0)\, c(w, a_2, l; 0, 0, 0), \end{aligned} \tag{2.18}$$

where

$$g_w(p', p) = \int_{-1}^{1} dx\, P_w(x)\, v(\sqrt{(p')^2 + p^2 - 2pp'x}), \tag{2.19}$$

with $P_w(x)$ being Legendre polynomials.

Finally, for the reaction on the deuteron we need only one isospin matrix element

$$\left\langle \left(\frac{1}{2}\frac{1}{2}\right) 1 - 1 \left| \frac{i}{\sqrt{2}} [(\boldsymbol{\tau}_1 \times \boldsymbol{\tau}_2)_x - i(\boldsymbol{\tau}_1 \times \boldsymbol{\tau}_2)_y] \right| \left(\frac{1}{2}\frac{1}{2}\right) 00 \right\rangle = 2, \tag{2.20}$$

while the missing 3N isospin matrix element to be used in the reactions with the 3N bound states is evaluated to

$$\left\langle \left(t'\frac{1}{2}\right)T'\,m_{T'}\left|\frac{i}{\sqrt{2}}\left[(\boldsymbol{\tau}_2\times\boldsymbol{\tau}_3)_x - i(\boldsymbol{\tau}_2\times\boldsymbol{\tau}_3)_y\right]\right|\left(t\frac{1}{2}\right)\frac{1}{2}\,m_T\right\rangle = 12\sqrt{3}\,\sqrt{(2t+1)\,(2t'+1)}\,(-1)^{t+\frac{3}{2}+T'}\begin{Bmatrix}1 & t & t'\\ \frac{1}{2} & T' & \frac{1}{2}\end{Bmatrix}$$
$$\times\begin{Bmatrix}1 & 1 & 1\\ \frac{1}{2} & \frac{1}{2} & t\\ \frac{1}{2} & \frac{1}{2} & t'\end{Bmatrix} c\left(1,\frac{1}{2},T';-1,m_T,m_T-1\right) \qquad (2.21)$$

and vanishes unless $t + t' = 1$.

III. RESULTS FOR THE $\pi^- + {}^2\mathrm{H} \to n + n$ AND $\pi^- + {}^3\mathrm{He} \to n + d$ REACTIONS

Recently, we investigated muon capture on ^{2}H, ^{3}He, and ^{3}H [76,77] as well as pion radiative capture in the same nuclei [82]. In the corresponding papers we described our momentum space framework and the way we calculate the initial and final nuclear states. We refer the reader especially to Appendices A and B of Ref. [82] for details. Since our framework is consistently nonrelativistic, we also analyzed effects stemming from approximate nonrelativistic treatment of kinematics. The kinematics of the pion absorption processes studied in the present paper is in fact simpler than for pion radiative capture and can be treated as a special case of it with the final photon energy zero. The initial state, including the K-shell pion, is the same. Thus we can be very brief and provide only few numbers, for the reader's orientation. Assuming the values for the proton, neutron, deuteron, ^{3}He, and negative pion masses, respectively, as $M_p = 938.272$ MeV, $M_n = 939.565$ MeV, $M_d = 1875.613$ MeV, $M_{^3\mathrm{He}} = 2808.392$ MeV, and $M_\pi = 139.57$ MeV, our (nonrelativistic) results for the magnitudes of the neutron momenta in the two-body pion absorption reactions are $p_0 = 357.534$ MeV ($\pi^- + {}^2\mathrm{H} \to n + n$) and $q_0 = 407.726$ MeV ($\pi^- + {}^3\mathrm{He} \to n + d$). We neglected the small atomic binding energy of the pion. The relativistic numbers are slightly (by approximately 2%) bigger.

Let us start with the $\pi^- + {}^2\mathrm{H} \to n + n$ reaction. The key ingredient of the absorption rate is here the nuclear matrix element of the transition operator $\rho = \rho(1) + \rho(2) + \rho(1,2)$ between the initial deuteron state and the final two-neutron scattering state. Introducing the spin magnetic quantum numbers m_d, m_1, m_2 for the deuteron, neutron 1 and neutron 2, respectively, we write

$$N_{nn}(m_1,m_2,m_d) = {}^{(-)}\langle \mathbf{p}_0 m_1 m_2\ \mathbf{P}_f = 0|\rho|\phi_d m_d\ \mathbf{P}_i = 0\rangle, \qquad (3.1)$$

where $|\mathbf{p}_0\, m_1\, m_2\ \mathbf{P}_f = 0\rangle^{(-)}$ denotes the 2N scattering state (see for example [80]).

Collecting all factors we arrive at the following expression for the total absorption rate in the $\pi^- + {}^2\mathrm{H} \to n + n$ reaction [89]:

$$\Gamma_{nn} = \frac{(\alpha\, M_d')^3\, c\, M_n\, p_0}{2M_{\pi^-}} \int d\hat{\mathbf{p}}_0\, \frac{1}{3} \sum_{m_1,m_2,m_d} |N_{nn}(m_1,m_2,m_d)|^2, \qquad (3.2)$$

where the phase-space factor, normalizations of the pion field and of the two-nucleon states, as well as the $\frac{(M_d'\alpha)^3}{\pi}$ factor stemming from the K-shell atomic wave function are taken into account with $M_d' = \frac{M_d M_{\pi^-}}{M_d + M_{\pi^-}}$ and $\alpha \approx \frac{1}{137}$ being the fine structure constant. The speed of light c is used to convert the units of Γ_{nn} from fm^{-1} to inverse seconds. We can further simplify (3.2), since for the unpolarized case there is no dependence on the direction of the neutron momentum $\hat{\mathbf{p}}_0$ and the integral over $d\hat{\mathbf{p}}_0$ yields 4π.

The results obtained with two different types of the two-nucleon potential, with different treatment of the final two-neutron state and the transition operator are collected in Table I. They show that the 2N contribution to the pion absorption operator changes the results (both PW and Full) obtained with the single-nucleon absorption operator by two to three orders of magnitude. Final-state interactions play an important role and their effects are especially strong in the calculations employing only the single-nucleon absorption operator. This conclusion is consistent with the previous studies of the time-reversed processes of meson production in NN collisions and of the reaction $NN \to NN\pi$, in particular, where the related NN initial-state interactions are known to play an important role [25,26].

The full results (SN + 2N, Full) calculated with the N^{4}LO$^+$ chiral NN wave functions show very good agreement with the experimental data. Predictions computed for the complete LO-MCS transition operator with $\Lambda = 450$ MeV at different chiral orders for the NN wave functions show good convergence. The spread of the complete results with the cutoff (measured by the standard deviation) is roughly two times smaller than for the corresponding (SN + 2N, PW) calculations. Clearly, the results for the softest cutoff $\Lambda = 400$ MeV slightly deviate from the others. Pion absorption is sensitive to intermediate momentum components of the wave function, which might not be properly represented in the wave functions computed with small cutoff values. Therefore, one might consider rejecting results obtained with the smallest Λ value. On the other hand, the cutoff dependence of the complete results stemming from the chiral NN wave functions at N^{4}LO$^+$ is much weaker than the expected LO-MCS theoretical uncertainty, even when the smallest cutoff is included. Indeed, using the expansion parameter for the production operator, $\chi \sim p/\Lambda_\chi \simeq 0.4$, where $\Lambda_\chi \simeq 4\pi f_\pi \simeq 1$ GeV is the chiral symmetry breaking scale, the theoretical uncertainty at the given order ν is expected to come from the first neglected chiral order $\nu + 1$ unless the coefficient in front of this term vanishes. Therefore, the theoretical uncertainty for

TABLE I. Absorption rates for the $\pi^- + {}^2\mathrm{H} \to n + n$ reaction calculated with the chiral semilocal momentum-space regularized two-nucleon force [83] at given chiral order (specified in column "chiral order in nuclear w.f.") and with particular cutoff values (column Λ) with the single-nucleon transition operator (SN) and including two-nucleon contributions (SN+2N) at leading order in the MCS (column "chiral order in production"). Plane wave results (PW) and results obtained with the inclusion of two-neutron rescattering (Full) are shown. The last column refers to the experimental value from the hadronic ground-state broadening in pionic deuterium [90,91].

			Absorption rate Γ_{nn} in 10^{15} s^{-1}				
			SN		SN+2N		Expt.
Chiral order in production	Chiral order in nuclear w.f.	Λ (MeV)	PW	Full	PW	Full	
LO-MCS	LO	450	0.0593	0.0883	3.541	3.613	
LO-MCS	NLO	450	0.0001	0.0135	2.221	2.059	
LO-MCS	N^{2}LO	450	0.0158	0.0039	1.827	1.433	
LO-MCS	N^{3}LO	450	0.0155	0.0087	1.836	1.237	$1.306^{+0.026}_{-0.055}$
LO-MCS	N^{4}LO	450	0.0131	0.0091	1.850	1.243	
LO-MCS	N^{4}LO$^+$	400	0.0028	0.0125	2.057	1.484	
LO-MCS	N^{4}LO$^+$	450	0.0142	0.0070	1.836	1.292	
LO-MCS	N^{4}LO$^+$	500	0.0305	0.0032	1.644	1.224	
LO-MCS	N^{4}LO$^+$	550	0.0460	0.0007	1.508	1.247	

the amplitude at the LO-MCS can be estimated as $\sim\chi$, which translates to $\sim 2\chi \simeq 80\%$ for the absorption rate, where the amplitude enters squared. It should, however, be stressed that there are no pion production operators involving pions and nucleons at next-to-leading order in the MCS (NLO-MCS), since all NLO-MCS operators from the loop diagrams were shown to cancel exactly in Ref. [41]. Also, as discussed in Ref. [44], there is a significant cancellation of the one-loop and tree-level diagrams involving the $\Delta(1232)$ at NLO-MCS. Therefore, the actual truncation uncertainty for the absorption rate on the deuteron is at least a factor of 2 smaller. We however keep this conservative uncertainty estimate for the absorption rates on heavier nuclei, since the cancellation of various $\Delta(1232)$ contributions might not be operative in such systems.

The results shown in Table I can be also compared with the state-of-the-art calculations of Refs. [41,44]. The cross section of the $p + p \to {}^2\mathrm{H} + \pi^+$ reaction in the center-of-mass system at threshold is conveniently parametrized as

$$\sigma = \alpha\eta, \tag{3.3}$$

where η is the outgoing pion momentum in the units of the pion mass. Using detailed balance, the absorption rate Γ_{nn} of the $\pi^- + {}^2\mathrm{H} \to n + n$ channel can be straightforwardly connected with the threshold parameter α in Eq. (3.3); see, e.g., Ref. [90] for details. This yields the experimental value from the hadronic ground-state broadening in pionic deuterium to be $\alpha = 251^{+5}_{-11}$ μb. Our LO-MCS calculation with the N^{4}LO$^+$ chiral wave functions gives $\alpha = \{283, 246, 233, 238\}$ μb for $\Lambda = \{400, 450, 500, 550\}$ MeV, in order. These results agree very well with the corresponding results of Refs. [41,44] obtained using modern phenomenological potentials. Therefore, we are now well prepared to make first EFT-based predictions for the absorption rates of more complicated pion capture reactions on ^{3}He and ^{3}H.

Let us now turn to the calculations of the absorption rate for the $\pi^- + {}^3\mathrm{He} \to n + d$ reaction. Pion absorption in ^{3}He was studied theoretically before in the early 1990s [92,93]. In [92] absorption of negative pions with energies between 42 and 256 MeV on ${}^1S_0$ proton pairs in ^{3}He was investigated in a model which included only partially the final-state interactions. The authors of [93] studied two-body pion absorption of stopped pions including various short-range absorption mechanisms but neglecting the nuclear distortion effects on the absorbed pions and the outgoing nucleons. Their work clearly showed the importance of the two-body terms in the pion absorption operator. In our formulation the crucial role is played by the matrix element of the 3N transition operator ρ_{3N},

$$N_{\mathrm{nd}}(m_n, m_d, m_{^3\mathrm{He}}) \equiv {}^{(-)}\langle \Psi_{\mathrm{nd}}\, m_n\, m_d\, \mathbf{P}_f = 0 | \rho_{3N} | \Psi_{^3\mathrm{He}}\, m_{^3\mathrm{He}}\, \mathbf{P}_i = 0 \rangle, \tag{3.4}$$

between the initial ^{3}He and the final two-cluster 3N scattering state with $\rho_{3N} = \rho(1) + \rho(2) + \rho(3) + \rho(2,3) + \rho(3,1) + \rho(1,2) + \rho(1,2,3)$, with the latter term neglected in this work, since its effects are expected to be beyond the accuracy level of our present calculations. Our formula for the total absorption rate reads

$$\Gamma_{\mathrm{nd}} = \mathcal{R}\, \frac{16\left(\alpha^3 M'_{^3\mathrm{He}}\right)^3 c\, M q_0}{9 M_{\pi^-}} \int d\hat{\mathbf{q}}_0 \times \frac{1}{2} \sum_{m_n, m_d, m_{^3\mathrm{He}}} |N_{\mathrm{nd}}(m_n, m_d, m_{^3\mathrm{He}})|^2, \tag{3.5}$$

where $M'_{^3\mathrm{He}} = \frac{M_{^3\mathrm{He}} M_{\pi^-}}{M_{^3\mathrm{He}} + M_{\pi^-}}$ is now the reduced mass of the π^--^{3}He system. We can use the same arguments as before to simplify the angular integrations. The final state energy is expressed in terms of the neutron momentum $\mathbf{q}_0$,

$$M_\pi + M_{^3\mathrm{He}} \approx M_n + M_d + \frac{3}{4}\frac{\mathbf{q}_0^{\,2}}{M}, \tag{3.6}$$

where we neglect the deuteron binding energy in the kinetic energy and use the average nucleon mass M. The factor $\mathcal{R} = 0.98$ is due to the finite volume of the ^{3}He charge [94].

TABLE II. Absorption rates for the $\pi^- + {}^3\mathrm{He} \to n + d$ reaction calculated with the chiral semilocal momentum-space regularized two-nucleon potentials [83] at $\mathrm{N^4LO^+}$ augmented by the consistently regularized three-nucleon force at $\mathrm{N^2LO}$ [84] for different values of the cutoff parameter (Λ). We compare four different calculations: (1) symmetrized plane wave with the single-nucleon and two-nucleon parts in the transition operator and three-nucleon force effects included in the initial three-nucleon bound state [PWIAS–(SN+2N)–(2NF+3NF)], (2) calculation with the initial and final states calculated with the same Hamiltonian comprising two- and three-nucleon forces but retaining only the single-nucleon contribution in the transition operator [Full–SN–(2NF+3NF)], (3) calculation with the initial and final states calculated with the same Hamiltonian comprising only two-nucleon forces and including the single-nucleon and two-nucleon parts in the transition operator [Full–(SN+2N)–2NF], and (4) calculation with the initial and final states calculated with the two- and three-nucleon forces and the complete transition operator [Full–(SN+2N)–(2NF+3NF)].

	Absorption rate Γ_{nd} in 10^{15} s^{-1}			
Λ (MeV)	Calc. (1)	Calc. (2)	Calc. (3)	Calc. (4)
400	8.3158	0.0172	3.6566	3.028
450	6.6961	0.0231	2.5466	2.089
500	5.4398	0.0666	1.9909	1.595
550	4.6015	0.1840	1.8029	1.371

(The corresponding factor in Γ_{nn} is very close to 1 [94] and therefore has not been included.)

Our results for Γ_{nd} are shown in Table II. We display there four different types of predictions obtained at $\mathrm{N^4LO^+}$ for four values of the parameter Λ: (1) symmetrized plane wave (PWIAS) with the single-nucleon and two-nucleon parts in the transition operator and three-nucleon force effects included in the initial three-nucleon bound state [PWIAS–(SN + 2N)–(2NF + 3NF)], (2) calculation with the initial and final states calculated with the same Hamiltonian comprising two- and three-nucleon forces but keeping only the single-nucleon contribution in the transition operator [Full–SN–(2NF + 3NF)], (3) calculation with the initial and final states calculated with the same Hamiltonian comprising only two-nucleon forces and including the single-nucleon and two-nucleon parts in the transition operator [Full–(SN + 2N)–2NF], and (4) calculation with the initial and final states calculated with the two- and three-nucleon forces and the complete transition operator [Full–(SN + 2N)–(2NF + 3NF)]. Thus by comparing calculations (2) and (4) we see the importance of the two-nucleon part of the transition operator. Also final state interactions play a significant role and reduce the rates approximately by a factor of three [calculations (1) vs (4)]. The three-nucleon force effects are clearly visible and grow with Λ amounting to more than 30% for $\Lambda = 550$ MeV [calculations (3) vs (4)]. The dependence of our most complete calculations (4) on the cutoff parameter Λ remains evident. This could be expected, since only LO MCS absorption operators are taken into account. Specifically, the cutoff dependence is expected to be significantly reduced when the two $NN \to NN\pi$ contact terms at NNLO-MCS will be taken into account.

TABLE III. Absorption rates for the $\pi^- + {}^3\mathrm{He} \to p + n + n$ reaction calculated with the same forces and with the same four types of dynamics as in the case of Γ_{nd} in Table II.

	Absorption rate Γ_{pnn} in 10^{15} s^{-1}			
Λ (MeV)	Calc. (1)	Calc. (2)	Calc. (3)	Calc. (4)
400	38.378	0.675	16.346	15.686
450	35.212	0.612	13.237	12.733
500	32.343	0.601	11.849	11.367
550	30.170	0.650	12.039	11.421

IV. RESULTS FOR THE $\pi^- + {}^3\mathrm{He} \to p + n + n$ AND $\pi^- + {}^3\mathrm{H} \to n + n + n$ REACTIONS

A. $\pi^- + {}^3\mathrm{He} \to p + n + n$

The kinematics of the three-body reactions in the center-of-mass frame requires in the unpolarized case two independent variables, and some choices are of special importance. We start with the one employed recently in muon capture and in pion radiative capture reactions with trinucleons [76,77,82], which utilizes the fact that the nuclear matrix element N_{pnn} is given in terms of the Jacobi momenta. For the $\pi^- + {}^3\mathrm{He} \to p + n + n$ reaction this key quantity is

$$N_{\mathrm{pnn}}(m_1, m_2, m_3, m_{^3\mathrm{He}}) \equiv {}^{(-)}\langle \Psi_{\mathrm{pnn}}\, m_1\, m_2\, m_3\, \mathbf{P}_f = 0 | \rho_{3N} | \Psi_{^3\mathrm{He}}\, m_{^3\mathrm{He}}\, \mathbf{P}_i = 0 \rangle, \tag{4.1}$$

and we use the following formula for the total absorption rate Γ_{pnn}:

$$\Gamma_{\mathrm{pnn}} = \mathcal{R}\, \frac{16\left(\alpha\, M'_{^3\mathrm{He}}\right)^3 c\, M}{9 M_{\pi^-}} \int d\hat{\mathbf{q}} \int_0^{2\pi} d\phi_p \int_0^{\pi} d\theta_p \sin\theta_p \times \int_0^{p_{\max}} dp\, p^2 \sqrt{\frac{4}{3}(M E_{pq} - p^2)}\, \frac{1}{2} \times \sum_{m_1, m_2, m_3, m_{^3\mathrm{He}}} |N_{\mathrm{pnn}}(m_1, m_2, m_3, m_{^3\mathrm{He}})|^2, \tag{4.2}$$

where the internal energy of the final 3N state E_{pq} is expressed in terms of the Jacobi relative momenta $\mathbf{p}$ and $\mathbf{q}$,

$$\mathbf{p} \equiv \tfrac{1}{2}(\mathbf{p}_2 - \mathbf{p}_3), \qquad \mathbf{q} \equiv \tfrac{2}{3}\left[\mathbf{p}_1 - \tfrac{1}{2}(\mathbf{p}_2 + \mathbf{p}_3)\right] = \mathbf{p}_1, \tag{4.3}$$

taking the form

$$M_\pi + M_{^3\mathrm{He}} \approx 3M + \frac{\mathbf{p}^2}{M} + \frac{3}{4}\frac{\mathbf{q}^2}{M} \equiv 3M + E_{pq} = 3M + \frac{p_{\max}^2}{M} = 3M + \frac{3}{4}\frac{q_{\max}^2}{M}. \tag{4.4}$$

For the unpolarized case we choose $\hat{\mathbf{q}} = \hat{\mathbf{z}}$ and $\phi_p = 0$, so the triple integral $\int d\hat{\mathbf{q}} \int_0^{2\pi} d\phi_p$ yields a factor of $8\pi^2$.

Our predictions for Γ_{pnn} are given in Table III for the same four types of calculations as in Table II. The crucial role played by the two-nucleon part of the transition operator is

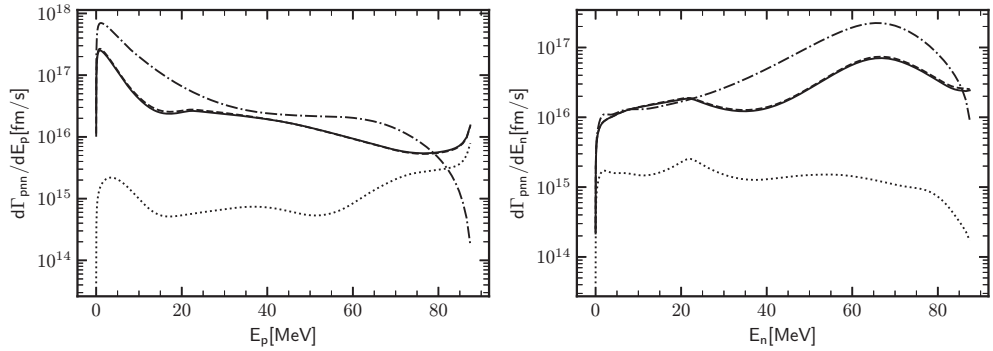

FIG. 2. Differential absorption rates $d\Gamma_{\rm pnn}/dE_p$ (left) and $d\Gamma_{\rm pnn}/dE_n$ (right) for the $\pi^- + {}^3{\rm He} \to p + n + n$ process, calculated using the SMS chiral potential at N^4LO^+ with $\Lambda = 450$ MeV and with the four different computational setups defined above: "PWIAS–(SN + 2N)–(2NF + 3NF)" (dash-dotted line), "Full–SN–(2NF + 3NF)" (dotted line), "Full–(SN + 2N)–2NF" (dashed line), "Full–(SN + 2N)–(2NF + 3NF)" (solid line).

proved also for this process calculations (2) vs (4)]. Final state interactions lower the rates by a factor of 2.5–2.8 [calculations (1) vs (4)]. The three-nucleon force effects are now much smaller and reach 5.5% for $\Lambda = 550$ MeV [calculations (3) vs (4)]. The relative spread of the results obtained with different Λ values is smaller than for the $\pi^- + {}^3{\rm He} \to n + d$ reaction and is further reduced by more than 2 if the prediction for the smallest $\Lambda = 400$ MeV is dropped.

Using the relation between the magnitudes of the Jacobi momenta from Eq. (4.4), we arrive at a new formula for $\Gamma_{\rm pnn}$,

$$\Gamma_{\rm pnn} = \mathcal{R}\,\frac{32\,\pi^2\left(\alpha\,M'_{^3{\rm He}}\right)^3 c\,M}{3M_{\pi^-}}\int_0^{\pi} d\theta_p \sin\theta_p \times \int_0^{q_{\rm max}} dq\,q^2\sqrt{ME_{pq}-\frac{3}{4}q^2} \times \frac{1}{2}\sum_{m_1,m_2,m_3,m_{^3{\rm He}}} |N_{\rm pnn}(m_1,m_2,m_3,m_{^3{\rm He}})|^2, \quad (4.5)$$

which is a good starting point to calculate the differential absorption rates $\frac{d\Gamma_{\rm pnn}}{dE_1}$, where nucleon 1 can be a proton or a neutron. Namely one simply reads out

$$\frac{d\Gamma_{\rm pnn}}{dq} = \frac{d\Gamma_{\rm pnn}}{dp_1} = \mathcal{R}\,\frac{32\,\pi^2\left(\alpha\,M'_{^3{\rm He}}\right)^3 c\,M}{3M_{\pi^-}}\,q^2 \times \sqrt{ME_{pq}-\tfrac{3}{4}q^2}\int_0^{\pi} d\theta_p \sin\theta_p \times \frac{1}{2}\sum_{m_1,m_2,m_3,m_{^3{\rm He}}} |N_{\rm pnn}(m_1,m_2,m_3,m_{^3{\rm He}})|^2. \quad (4.6)$$

In Fig. 2 we show our predictions for the single-nucleon spectra $\frac{d\Gamma_{\rm pnn}}{dE_1} = \frac{M}{p_1}\frac{d\Gamma_{\rm pnn}}{dp_1}$ obtained with the four types of dynamics to show the role of the 2N contributions in the transition operator ρ_{3N} and study the 3N force effects. Similarly to Tables II and III, we see in Fig. 2 that calculations employing only the single-nucleon pion absorption operator yield much lower values of the absorption rate. It is also visible that the rescattering part of the nuclear matrix element plays an important role as its inclusion reduces significantly the PWIAS predictions for $\frac{d\Gamma_{\rm pnn}}{dE_p}$ as well as for $\frac{d\Gamma_{\rm pnn}}{dE_n}$ and changes their shape, making it more complicated. In particular the PWIAS results do not exhibit any enhancement in the vicinity of the maximal proton energy. On the other hand 3N force effects are rather small and are hardly visible on a logarithmic scale: the dashed and solid lines practically overlap.

The exclusive results for the $\pi^- + {}^3{\rm He} \to p + n + n$ reaction can be demonstrated in the form of double differential absorption rates. One of the possible choices is $d^2\Gamma_{\rm pnn}/(dE_1\,dE_2)$, calculated as

$$\frac{d^2\Gamma_{\rm pnn}}{dE_1\,dE_2} = \mathcal{R}\,\frac{64\,\pi^2\left(\alpha\,M'_{^3{\rm He}}\right)^3 c\,M^3}{3M_{\pi^-}} \times \frac{1}{2}\sum_{m_1,m_2,m_3,m_{^3{\rm He}}} |N_{\rm pnn}(m_1,m_2,m_3,m_{^3{\rm He}})|^2, \quad (4.7)$$

in the (E_1, E_2) domain, where $-1 \leqslant \frac{E-2E_1-2E_2}{2\sqrt{E_1E_2}} \leqslant 1$. Here $E \equiv E_{pq}$ is the total kinetic 3N energy

$$E = E_1 + E_2 + E_3. \quad (4.8)$$

We can also introduce dimensionless variables x and y as

$$x = \sqrt{3}\,(E_1 + 2E_2 - E)/E, \qquad y = (3E_1 - E)/E, \quad (4.9)$$

restricted to the disk $r^2 \equiv x^2 + y^2 \leqslant 1$ and evaluate $d^2\Gamma_{\rm pnn}/(dx\,dy)$ or (using polar coordinates) $d^2\Gamma_{\rm pnn}/(dr\,d\phi)$. Such forms were used for example in Ref. [65].

In Fig. 3 we show the $d^2\Gamma_{\rm pnn}/(dE_1 dE_2)$ obtained within the same dynamical models as used in Fig. 2 for the cutoff value $\Lambda = 450$ MeV. Our most advanced prediction "Full–(SN + 2N)–(2NF + 3NF)" is given in the right bottom panel. The dominant contributions to this double differential capture rate stem from configurations close to the borders of the kinematically allowed region. This could be expected as some special kinematical configurations are located there. For the nucleon-induced deuteron breakup process, where there are three free nucleons in the final state, the differential cross

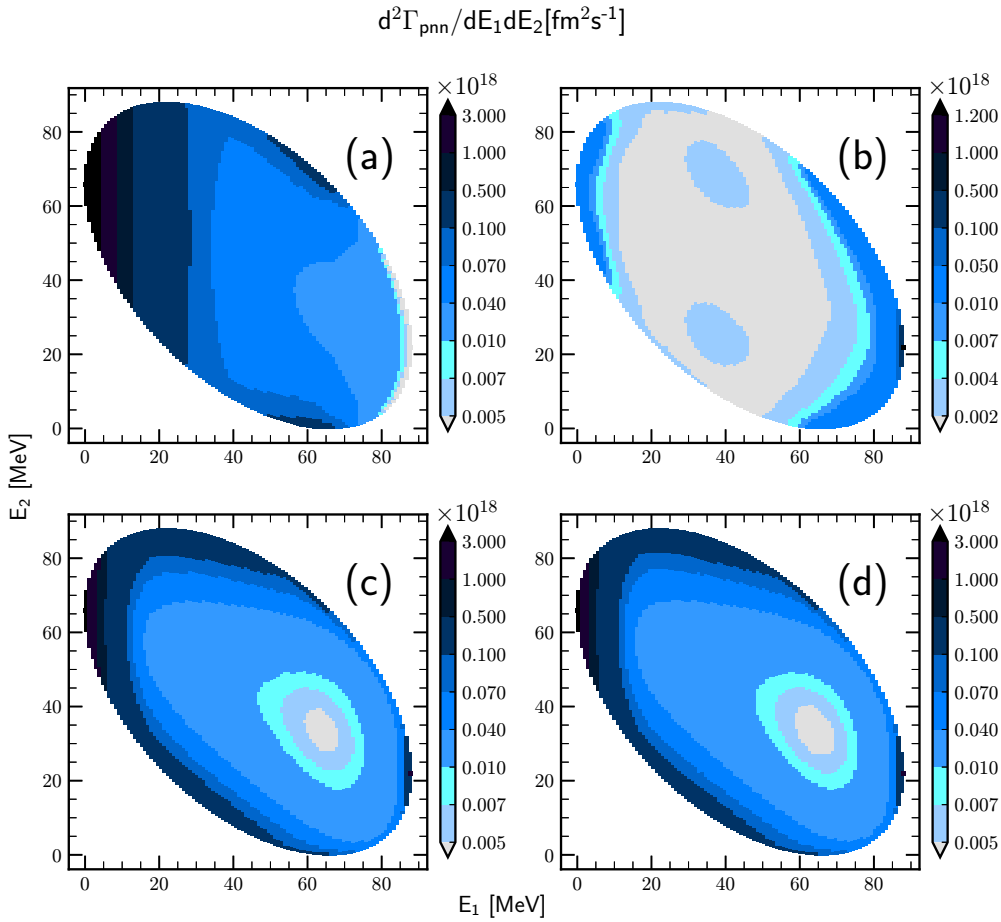

FIG. 3. Intensity plots for the double differential absorption rates $d^2\Gamma_{\rm pnn}/(dE_1dE_2)$ for the $\pi^- + {}^3\mathrm{He} \to p + n + n$ process, obtained using the SMS chiral potential at $\mathrm{N^4LO^+}$ with $\Lambda = 450$ MeV in the four computational setups defined above: "PWIAS–(SN + 2N)–(2NF + 3NF)" (a), "Full–SN–(2NF + 3NF)" (b), "Full–(SN + 2N)–2NF" (c), "Full–(SN + 2N)–(2NF + 3NF)" (d). Nucleon 1 is a proton.

section is enhanced in specific kinematical configurations [73]. We observe the same phenomenon in the pion absorption differential rates discussed here. The first type of important configurations is related to a strong final state interaction between two nucleons emerging with zero or very small relative energy. In the neutron-neutron final state interaction [FSI(nn)] configuration the proton (particle 1) gets two-thirds of the available kinetic energy and each neutron one-sixth of it, with $\mathbf{p}_1 = -2\mathbf{p}_2 = -2\mathbf{p}_3$. Rescattering effects at the FSI(nn) kinematics increase the capture rates significantly, from 9.7×10^{14} fm^{2}s^{-1} to 2.36×10^{18} fm^{2}s^{-1}. This is seen when comparing left upper and right bottom plots, for which predictions differ only in taking FSI into account. A rapid drop of the $d\Gamma_{\rm pnn}/dE_p$ at high values of E_1 also appears on Fig. 2 (left). The change of the capture rates for the two proton-neutron final state interaction kinematical configurations [FSI(pn)] located on the graphs at maximal E_2 and the diagonal $E_1 = E_2$ for the lowest allowed energies ($\approx$23 MeV) is smaller. For example, for FSI(pn) at $E_2 = 87.46$ MeV "PWIAS–(SN + 2N)–(2NF + 3NF)" capture rate $d^2\Gamma_{\rm pnn}/(dE_1dE_2)$ is 1.5×10^{17} fm^{2}s^{-1} while the "Full–(SN + 2N)–(2NF + 3NF)" capture rate amounts to 4.48×10^{17} fm^{2}s^{-1}. The other interesting kinematical configurations located on the border of kinematically allowed region correspond to quasifree scattering (QFS), where two nucleons share equally the absorbed energy, while the third (spectator) nucleon remains at rest. Obviously, two such configurations are located at $E_1 = 0$ MeV [QFS(nn)] and at $E_2 = 0$ [QFS(pn)]. The remaining QFS(pn) configuration is located at the diagonal $E_1 = E_2$ for the highest allowed energies ($\approx$68 MeV). Here effects of the FSI are less pronounced and change the absorption rates up to 17%. The absorption rate $d^2\Gamma_{\rm pnn}/(dE_1dE_2)$ reaches its maximum just for the QFS(nn) configuration.

A comparison of the results shown in the right column of Fig. 3 brings information on the role of the two-nucleon components of the pion absorption operator. The capture rates obtained with the single nucleon absorption operator only are definitely smaller than those obtained in the "Full–(SN + 2N)–(2NF + 3NF)" model, and the "Full–SN–(2NF + 3NF)" total capture rate receives nearly all non-negligible contributions from configurations with low or high E_1 energies.

Finally, by comparing two plots in the bottom row of Fig. 3 we demonstrate that three-body forces do not play a significant role in this process. Since inclusion of a three-nucleon force in the bound state calculations changes the ^{3}He wave function, this comparison might suggest that the $\pi^- + {}^3\mathrm{He} \to$

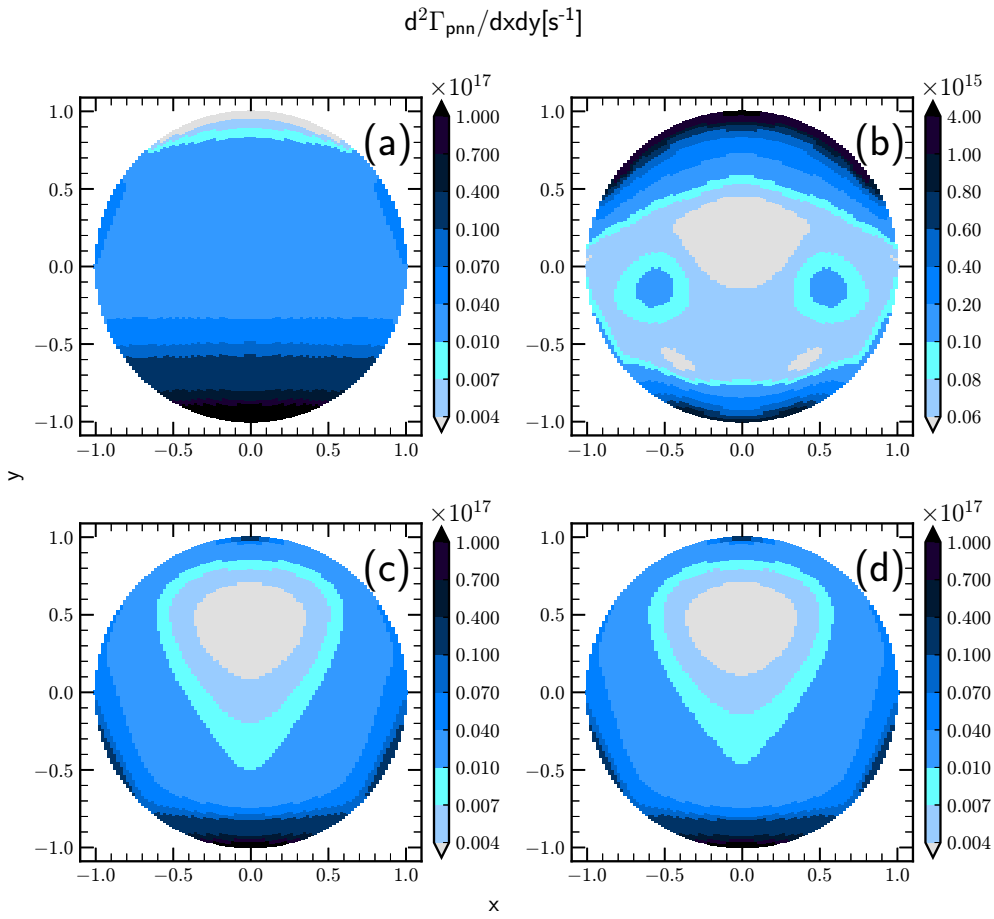

FIG. 4. Intensity plots for the double differential absorption rates $d^2\Gamma_{\rm pnn}/(dx\,dy)$ for the $\pi^- + {}^3\mathrm{He} \to p + n + n$ process, obtained using the SMS potential at $\mathrm{N^4LO^+}$ with $\Lambda = 450$ MeV in the four different computations defined above: "PWIAS–(SN + 2N)–(2NF + 3NF)" (a), "Full–SN–(2NF + 3NF)" (b), "Full–(SN + 2N)–2NF" (c), "Full–(SN + 2N)–(2NF + 3NF)" (d). Nucleon 1 is a proton.

$p + n + n$ reaction is rather insensitive to details of the nuclear bound state.

Obviously, the same observations arise from Fig. 4, where we show the double differential absorption rates $d^2\Gamma_{\rm pnn}/(dx\,dy)$. Here, the FSI($nn$) configuration is placed at $(x, y) = (0, 1)$ and the two FSI(pn) configurations are positioned on the border of the kinematically allowed region at an angle of 120° from FSI(nn) point symmetrically: clockwise and counterclockwise. In the (x, y) representation the QFS(nn) configuration is located at $(x, y) = (0, -1)$ and again the angles corresponding to the two QFS(pn) configurations differ from the QFS(nn) angle by $\pm 120°$. The results in the right bottom panel of Fig. 4 highlight even better the importance of the above mentioned special configurations than the representation used in Fig. 3. The "Full–SN–(2NF + 3NF)" model delivers the absorption rate approximately two orders of magnitude smaller than the predictions based on the single-nucleon absorption operator supplemented by two-nucleon operators. The expected left-right symmetry seen in all panels of Fig. 4 confirms the high accuracy of our numerical methods.

Since the intensity plots (Figs. 3 and 4) suggest that $\Gamma_{\rm pnn}$ receives dominant contributions from the regions in the vicinity of the boundaries, in Fig. 5 we show also the differential absorption rate $d\Gamma_{\rm pnn}/dr$. Indeed, for all approaches, including even the PWIAS ones, the dominant contribution to the total absorption rate $\Gamma_{\rm pnn}$ arises from the narrow ring with $r > 0.9$, while the contributions coming from the central region ($r \lesssim 0.1$) are four orders of magnitude smaller. Note however, that, in accordance with Fig. 4, for the "PWIAS–(SN + 2N)–(2NF + 3NF)," the "Full–SN–(2NF + 3NF)," and the "Full–(SN + 2N)–(2NF + 3NF)" approaches the highest absorption rates are located at different parts of the ring $r > 0.9$.

In Ref. [65] the authors considered the two-dimensional distribution of experimental events in the narrow ring near the boundary of the kinematically allowed region defined by $0.95 \leqslant r \leqslant 1$. We thus calculate the corresponding quantity $d\Gamma^{\rm ring}_{\rm pnn}/d\Phi = \int_{0.95}^{1} dr\, d\Gamma_{\rm pnn}/(dr\, d\Phi)$ and show the results in Fig. 6. The angle Φ is measured clockwise from the point $(x = 0,\ y = 1)$, where E_1 has the maximal value $E_1 = \frac{2}{3}E$ and $E_2 = E_3 = \frac{1}{6}E$. This corresponds to the final state interaction kinematics where $\mathbf{p}_2 = \mathbf{p}_3 = -\frac{1}{2}\mathbf{p}_1$. The angular dependence of the $d\Gamma^{\rm ring}_{\rm pnn}/d\Phi$ changes with the dynamical approach used. Specifically, the model employing only the single nucleon pion absorption operator predicts the dominant contribution

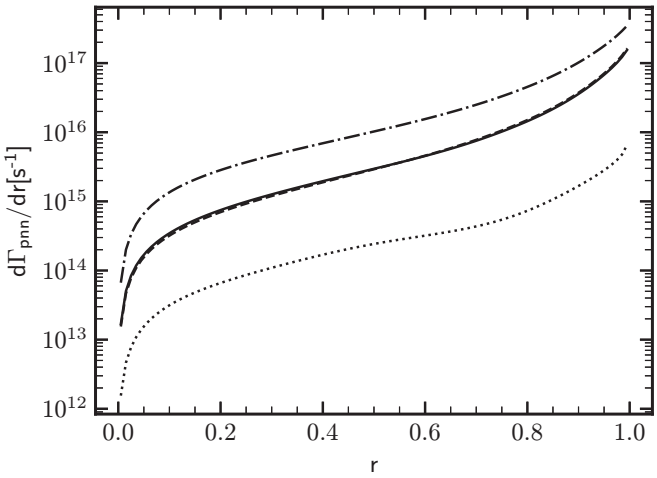

FIG. 5. Differential absorption rate $d\Gamma_{\rm pnn}/dr$ for the $\pi^- + {}^3\mathrm{He} \to p + n + n$ process, calculated using the SMS potential at $\mathrm{N^4LO^+}$ with $\Lambda = 450$ MeV and with the four dynamical setups defined above: "PWIAS–(SN + 2N)–(2NF + 3NF)" (dash-dotted line), "Full–SN–(2NF + 3NF)" (dotted line), "Full–(SN + 2N)–2NF" (dashed line), "Full–(SN + 2N)–(2NF + 3NF)" (solid line). Nucleon 1 is a proton.

from the vicinity of the FSI(nn) configuration (low Φ), while for the PWIAS model the absorption rate in question has minimal values at low Φ and rises more than 1000 times to achieve a maximum at $\Phi = 180^\circ$ [region close to the QFS(pn) configuration]. For the two remaining models the $d\Gamma^{\rm ring}_{\rm pnn}/d\Phi$ has maxima both at low and high Φ; however, the latter

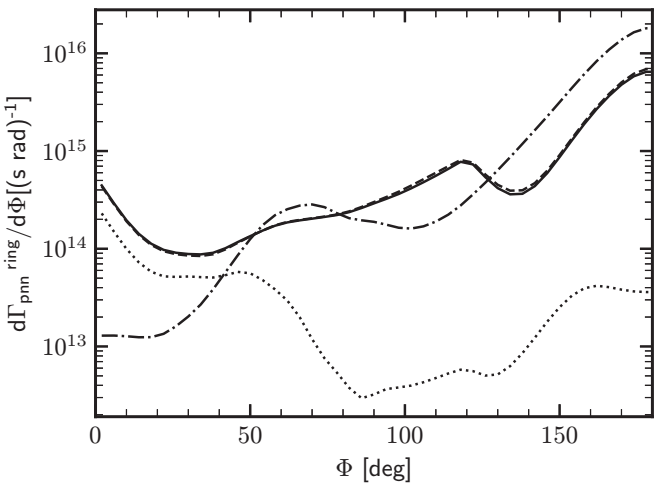

FIG. 6. Angular distribution of the differential absorption rate $d\Gamma^{\rm ring}_{\rm pnn}/d\Phi$ for the $\pi^- + {}^3\mathrm{He} \to p + n + n$ process, calculated using the SMS chiral potential with $\Lambda = 450$ MeV and with the four dynamical setups defined above: "PWIAS–(SN + 2N)–(2NF + 3NF)" (dash-dotted line), "Full–SN–(2NF + 3NF)" (dotted line), "Full–(SN + 2N)–2NF" (dashed line), "Full–(SN + 2N)–(2NF + 3NF)" (solid line). Nucleon 1 is a proton and due to the symmetry of the problem the angular distribution is shown in the interval $0 \leqslant \Phi \leqslant 180^\circ$.

TABLE IV. Absorption rates in the four regions of the phase space I_i defined in Ref. [65] for the $\pi^- + {}^3\mathrm{He} \to p + n + n$ reaction calculated with the chiral semilocal momentum-space regularized two-nucleon potentials [83] at $\mathrm{N^4LO^+}$ augmented by the consistently regularized three-nucleon force at $\mathrm{N^2LO}$ [84] with different values of the cutoff parameter Λ. The rates are determined with the two- and three-nucleon forces and the complete transition operator [Full–(SN+2N)–(2NF+3NF)].

	Absorption rates Γ_i in 10^{15} s^{-1}			
Λ (MeV)	I_1	I_2	I_3	I_4
400	9.463	1.789	0.340	0.185
450	7.614	1.452	0.308	0.179
500	6.758	1.298	0.299	0.176
550	6.826	1.302	0.309	0.173

maximum is around one order of magnitude higher. A local maximum seen at $\Phi = 120^\circ$ is related to the FSI(pn) region.

In Ref. [65] the authors consider four regions, I_1, I_2, I_3, and I_4, in the phase space of the $\pi^- + {}^3\mathrm{He} \to p + n + n$ process, which are defined in Fig. 14 and Table III of their paper. The regions were determined in terms of the Φ angles of the Dalitz plot and we could calculate, with various dynamics, the corresponding parts (denoted by Γ_i) of the total absorption rates $\Gamma_{\rm pnn}$. Our predictions for the most consistent dynamics are presented in Table IV.

In order to compare our results with [65] and avoid normalization issues we put in Table V the same results as in Table IV but normalized by the sum over all regions I_i. The same normalization is applied to the experimental results from the paper and listed in the same table. In such a way we do not compare the absolute values of the partial absorption rates, but their relative values. One can see that most of the regions have values comparable to the experimental results. The biggest inconsistency is found for the region I_2, while the best agreement emerges for the region I_3. For the normalized values the dependence on the cutoff value Λ gets weaker, which means that the choice of the cutoff affects more strongly the absolute values of the absorption rate than its distribution over the available phase space.

Our results for the $\Gamma_{\rm nd}$ and $\Gamma_{\rm pnn}$ rates were calculated by explicit summation (integration) over the two- and three-body nuclear states. We can also employ the method which uses

TABLE V. The same as in IV but all the values are normalized by the sum $I_1 + I_2 + I_3 + I_4$. The experimental results from Ref. [65] shown in the table are also normalized in the same way.

	Normalized absorption rates Γ_i			
Λ (MeV)	I_1	I_2	I_3	I_4
400	0.804	0.152	0.029	0.016
450	0.797	0.152	0.032	0.019
500	0.792	0.152	0.035	0.021
550	0.793	0.151	0.036	0.020
Gotta *et al.* [65]	0.844	0.099	0.033	0.023

TABLE VI. Absorption rates Γ_{nd}, Γ_{pnn}, and their sum $\Gamma_{nd}+\Gamma_{pnn}$, compared to the result $\Gamma^{closure}_{^3He}$, obtained using the closure method described in Ref. [82] for negative pion absorption in ^{3}He calculated with the chiral semilocal momentum-space regularized two-nucleon potentials [83] at N^{4}LO$^+$ augmented by the consistently regularized three-nucleon force at N^{2}LO [84] with different values of the cutoff parameter Λ. The initial and final states are computed with the two- and three-nucleon forces and the complete transition operator is employed [Full–(SN+2N)–(2NF+3NF)].

	Absorption rates in 10^{15} s^{-1}			
Λ (MeV)	Γ_{nd}	Γ_{pnn}	$\Gamma_{nd}+\Gamma_{pnn}$	$\Gamma^{closure}_{^3He}$
400	3.028	15.686	18.714	18.490
450	2.089	12.733	14.822	14.621
500	1.595	11.367	12.961	12.772
550	1.371	11.421	12.792	12.598

closure [82] and allows us to determine the total absorption rate, which should agree with $\Gamma_{nd}+\Gamma_{pnn}$. This important numerical check for our most complete dynamics is shown in Table VI. The obtained agreement is in general very good and the differences of predictions obtained within the two methods remain below 1.5%. Such an accuracy level of our numerical calculations was estimated in [73].

The results shown in Table VI can be summarized as follows:

$$\Gamma_{nd} = \left(2.0^{+1.0}_{-0.6} \pm 1.6\right) \times 10^{15}\ \text{s}^{-1} \tag{4.10}$$

$$\Gamma_{pnn} = \left(12.8^{+2.9}_{-1.4} \pm 10.2\right) \times 10^{15}\ \text{s}^{-1} \tag{4.11}$$

$$\Gamma_{nd}+\Gamma_{pnn} = \left(14.8^{+3.9}_{-2.0} \pm 11.8\right) \times 10^{15}\ \text{s}^{-1}, \tag{4.12}$$

where the central value and the first (asymmetric) uncertainty correspond to the average and the spread of the results in Table VI from the cutoff variation, while the second error is related to the truncation of the chiral expansion at the LO-MCS.

Absolute rates for different absorption channels in ^{3}He are also available from experiments. The broadening of the ground state level of the $\pi^-\,^3$He atom measured in the x-ray transitions $np \to 1s$ reads [62] (see also Ref. [95] for an older measurement)

$$\Gamma_{1s} = (28 \pm 7)\text{eV} = (43 \pm 11) \times 10^{15}\ \text{s}^{-1}. \tag{4.13}$$

Further, branching ratios for the channels $\pi^- + {}^3\text{He} \to n+d$ and $\pi^- + {}^3\text{He} \to p+n+n$ were measured to be $(16 \pm 2)\%$ [63,64] and $(58 \pm 5)\%$ [63], respectively. The sum of these two channels was also measured indirectly to be $(68.2 \pm 2.6)\%$ [96]. Using this information, one can extract the individual and combined contributions to the absorption rate on ^{3}He, which read

$$\Gamma^{exp.}_{nd} = (6.8 \pm 1.9) \times 10^{15}\ \text{s}^{-1} \tag{4.14}$$

$$\Gamma^{exp.}_{pnn} = (24.7 \pm 6.5) \times 10^{15}\ \text{s}^{-1} \tag{4.15}$$

$$\Gamma^{exp.}_{nd+pnn} = (29.0 \pm 7.3) \times 10^{15}\ \text{s}^{-1}. \tag{4.16}$$

TABLE VII. Absorption rates for the $\pi^- + {}^3\text{H} \to n+n+n$ reaction calculated with the same combinations of 2N and 3N potentials and with the same four types of dynamics as in the case of Γ_{nd}.

	Absorption rate Γ_{nnn} in 10^{15} s^{-1}			
Λ (MeV)	Calc. (1)	Calc. (2)	Calc. (3)	Calc. (4)
400	2.352	0.086	1.360	1.375
450	2.264	0.074	1.103	1.110
500	2.179	0.065	0.999	1.002
550	2.120	0.057	1.056	1.061

While our central values are clearly smaller than the experimental one, our results are still generally consistent with the data within errors. Future studies should show if agreement with the data improves when higher-order production operators are included.

B. $\pi^- + {}^3\text{H} \to n+n+n$

The formula for the total absorption rate Γ_{nnn} in the case of the $\pi^- + {}^3\text{H} \to n+n+n$ reaction,

$$\Gamma_{nnn} = \frac{2\left(\alpha\, M'_{^3\text{H}}\right)^3 c\, M}{27 M_{\pi^-}} \int d\hat{\mathbf{q}} \int_0^{2\pi} d\phi_p \int_0^{\pi} d\theta_p \sin\theta_p \times \int_0^{p_{\max}} dp\, p^2 \sqrt{\frac{4}{3}(ME_{pq} - p^2)} \times \frac{1}{2} \sum_{m_1,m_2,m_3,m_{^3\text{H}}} |N_{nnn}(m_1, m_2, m_3, m_{^3\text{He}})|^2, \tag{4.17}$$

is very similar to the one in Eq. (4.2); obviously it contains the appropriate matrix element

$$N_{nnn}(m_1, m_2, m_3, m_{^3\text{H}}) \equiv {}^{(-)}\langle \Psi_{nnn}\, m_1\, m_2\, m_3\, \mathbf{P}_f = 0 | \rho_{3N} | \Psi_{^3\text{H}}\, m_{^3\text{H}}\, \mathbf{P}_i = 0 \rangle, \tag{4.18}$$

an altered factor $\frac{1}{2} \to \frac{1}{6}$ due the three identical particles in the final state, as well as the proper reduced mass of the $\pi^- - {}^3\text{H}$ system, $M'_{^3\text{H}} = \frac{M_{^3\text{H}} M_{\pi^-}}{M_{^3\text{H}} + M_{\pi^-}}$. The $\mathcal{R}$ factor is very close to 1 and thus is unnecessary for this nucleus.

Results of our calculations for Γ_{nnn} at N^{4}LO$^+$ with different cutoff values and for the same four types of calculations as for Γ_{pnn} are given in Table VII. For all the four computations one can observe variations depending on the cutoff value; the maximal difference is for the "Full–SN–(2NF + 3NF)" [calc. (2)] and is up to 34% while the smallest cutoff dependence is for "PWIAS–(SN + 2N)–(2NF + 3NF)" [calc. (1)]; less then 10%. For each cutoff value the changes between different types of calculations remain similar: the rescattering part of the nuclear matrix element and the 2N contribution to the absorption operator are clearly important and have a very strong influence on the final value. On the other hand, inclusion of 3NF does not change the predictions substantially. The

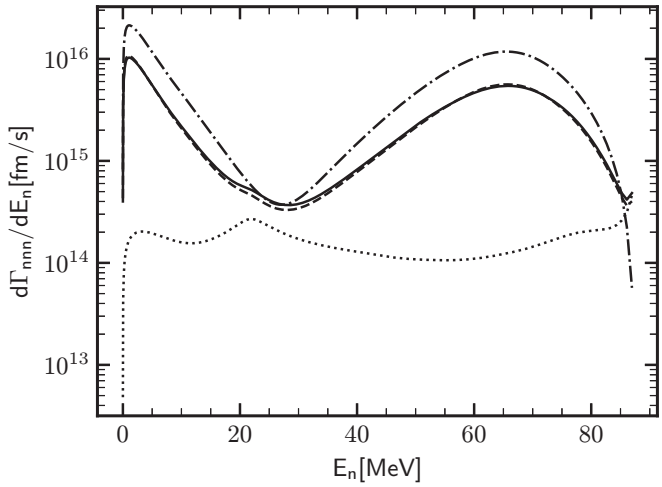

FIG. 7. The same as in Fig. 2 for the neutron spectrum $d\Gamma_{\rm nnn}/dE_n$ in the $\pi^- + {}^3\mathrm{H} \to n + n + n$ process.

summary of the complete results [calc. (4)] can be read as

$$\Gamma_{\rm nnn} = \left(1.1^{+0.2}_{-0.1} \pm 0.9\right) \times 10^{15}\ \mathrm{s}^{-1}, \qquad (4.19)$$

where, as before, we averaged over the four cutoff values and added the truncation uncertainty at the LO-MCS.

In Fig. 7 we show, in analogy to Fig. 2, the differential absorption rates $d\Gamma_{\rm nnn}/dE_n$. The structure of the pion absorption operator has a decisive influence on the observed spectrum. For most of the energies inclusion of two-body absorption operators increases the absorption rate by about two orders of magnitude. The other predictions are more compatible with each other. The "PWIAS–(SN + 2N)–(2NF + 3NF)" results are much bigger than the others (by a factor of 2–5) and reach their minima both at the neutron's lowest and highest energy. The "Full–(SN + 2N)–2NF" and "Full–(SN + 2N)–(2NF + 3NF)" predictions practically overlap. All predictions comprising the final state interactions exhibit a sudden enhancement of the absorption rate at the right limit of the spectrum.

Following the path used for the pion absorption on ^{3}He, in Figs. 8 and 9 we show the absorption rates $d^2\Gamma_{\rm nnn}/(dE_1 dE_2)$ and $d^2\Gamma_{\rm nnn}/(dx\,dy)$, respectively. The symmetry of presented plots is, of course, due to three indistinguishable neutrons in the final state. With the exception of the "Full–SN–(2NF + 3NF)" predictions, the dominant contributions to the absorption rates come exclusively from the three QFS(nn) configurations. The inclusion of the rescattering effects or the three-nucleon interaction does not change this picture and only slightly modifies magnitudes of the

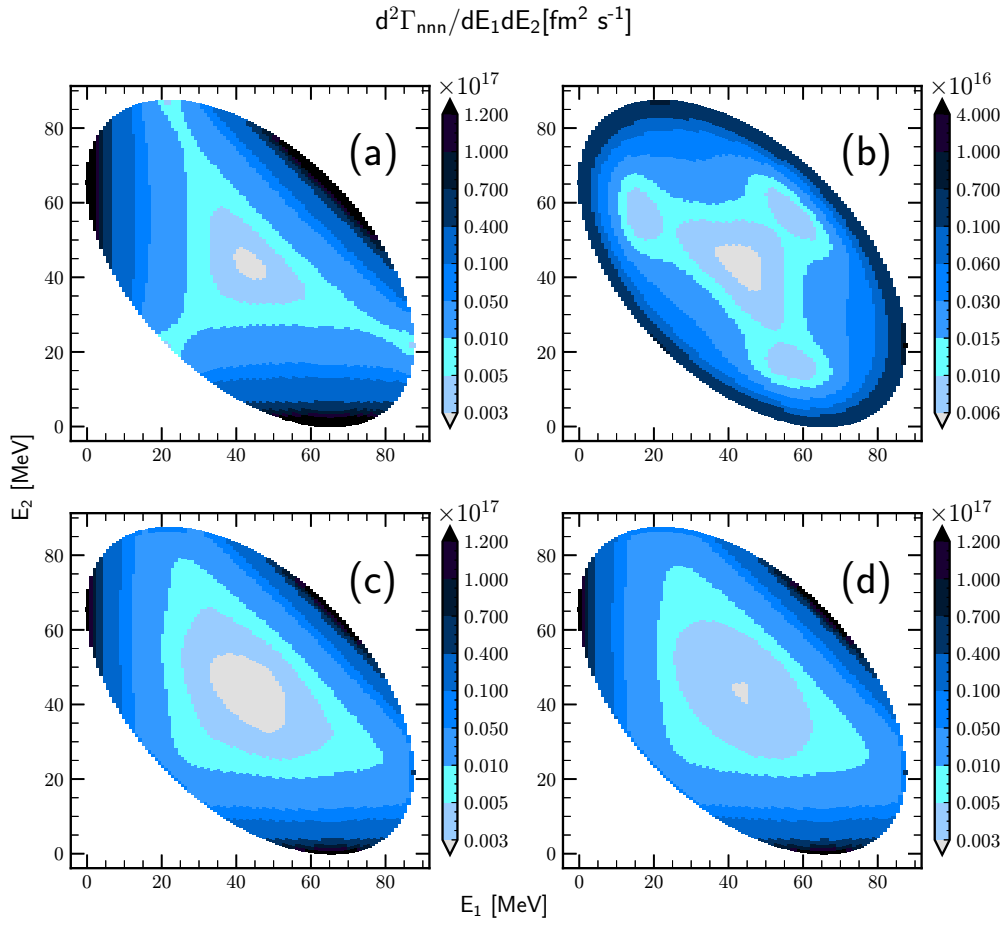

FIG. 8. The same as in Fig. 3 for the double differential absorption rates $d^2\Gamma_{\rm nnn}/(dE_1 dE_2)$ for the $\pi^- + {}^3\mathrm{H} \to n + n + n$ process.

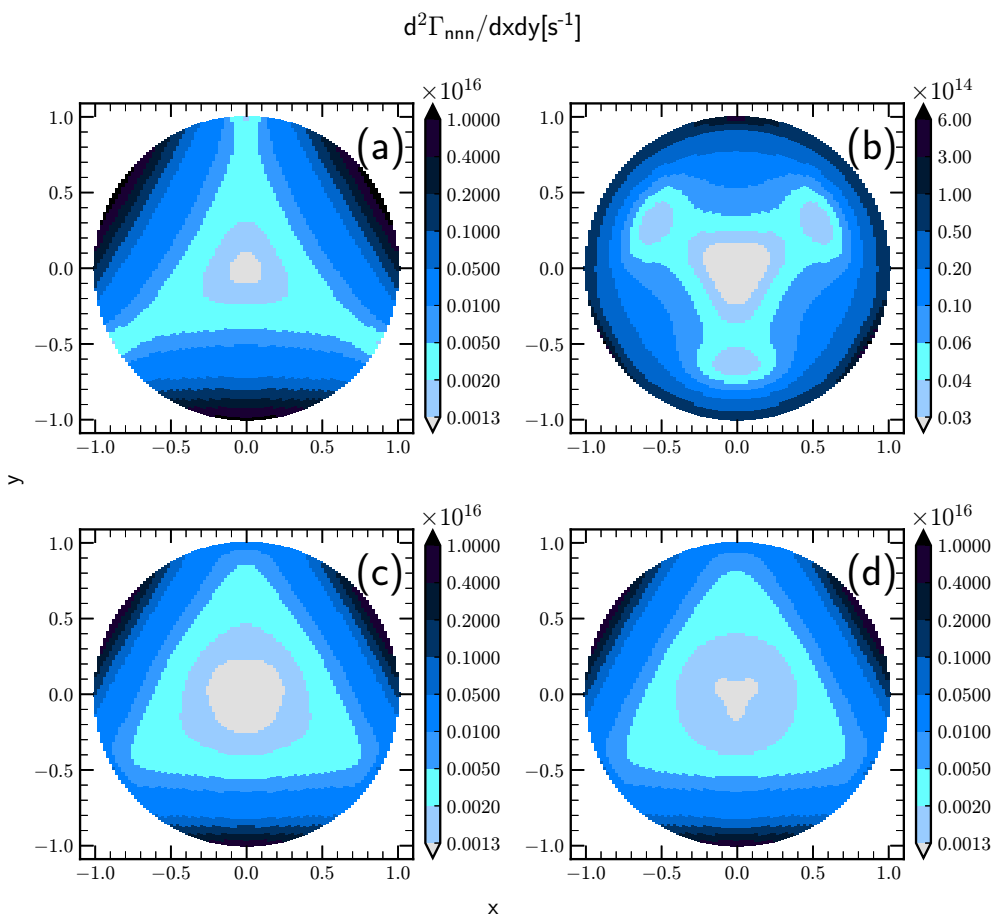

FIG. 9. The same as in Fig. 4 for the double differential absorption rates $d^2\Gamma_{nnn}/(dx\,dy)$ for the $\pi^- + {}^3\mathrm{H} \to n + n + n$ process.

absorption rates. For the QFS(nn) the differential absorption rate $d^2\Gamma_{nnn}/(dE_1 dE_2)$ changes from 4.3×10^{17} for the "PWIAS–(SN + 2N)–(2NF + 3NF)," 6.05×10^{16} for the "Full–SN–(2NF + 3NF)," and 2.24×10^{17} for "Full–(SN + 2N)–2NF" to 2.09×10^{17} for the most complete "Full–(SN + 2N)–(2NF + 3NF)" prediction (all values in $\mathrm{fm}^2\mathrm{s}^{-1}$). In the case of the FSI(nn) configuration we observe only a moderate increase of the absorption rates when the the final state interactions are included.

The integrated spectra in polar coordinates for the $\pi^- + {}^3\mathrm{H} \to n + n + n$ absorption rates $d\Gamma_{nnn}/dr$ and $d\Gamma^{\mathrm{ring}}_{nnn}/d\Phi$ are given in Figs. 10 and 11, respectively. Qualitatively, the picture resembles those for $\pi^- + {}^3\mathrm{He} \to p + n + n$ process: the single-nucleon absorption operator based predictions lie much below the other ones, the PWIAS results are above those taking rescattering among the three outgoing nucleons into account, and 3NF plays no significant role. Both figures highlight a dominant role of the QFS(nn) configuration.

Finally, our results for the Γ_{nnn} rates are compared in Table VIII with the corresponding predictions $\Gamma^{\mathrm{closure}}_{^3\mathrm{H}}$ obtained using the closure approach. The difference between these two results is very small and does not exceed 0.2%. The agreement is even more evident than for the total pion absorption rate in ^{3}He. The reason for the better agreement in the ^{3}H case might be that, contrary to ^{3}He, here we deal with only one, three-body breakup channel. The results confirm the consistence between the three-nucleon bound and scattering states calculated without and with the inclusion of the 3N potential.

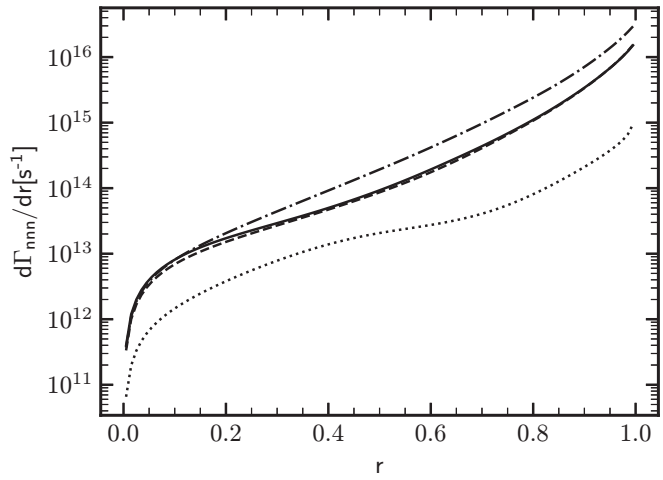

FIG. 10. The same as in Fig. 5 for the $\pi^- + {}^3\mathrm{H} \to n + n + n$ process.

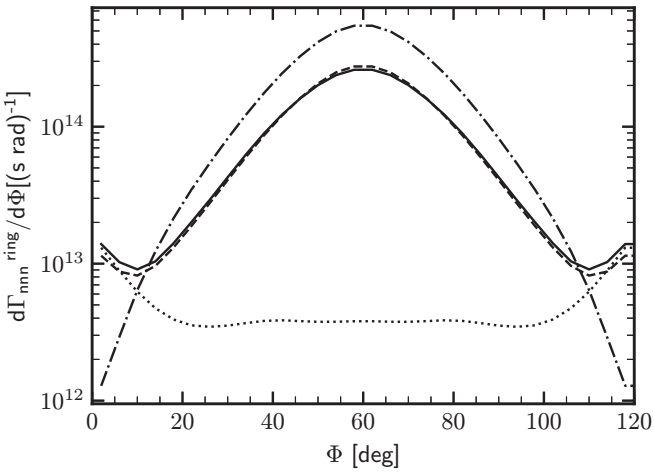

FIG. 11. The same as in Fig. 6 for the $\pi^- + {}^3\mathrm{H} \to n + n + n$ process, The angular distribution inside the ring is shown $d\Gamma_{nnn}^{ring}/d\Phi$ only in the interval $0 \leqslant \Phi \leqslant 120^\circ$ due to the symmetry of the problem.

V. SUMMARY AND OUTLOOK

We investigated the $\pi^- + {}^2\mathrm{H} \to n + n$, $\pi^- + {}^3\mathrm{H} \to n + n + n$, $\pi^- + {}^3\mathrm{He} \to n + d$ and $\pi^- + {}^3\mathrm{He} \to p + n + n$ capture reactions from the lowest atomic orbitals under full inclusion of final state interactions. In the calculations we employed the LO single-nucleon and two-nucleon transition operators [26] derived using momentum counting scheme within chiral effective field theory. The nuclear states were obtained with the chiral semilocal momentum-space regularized two-nucleon forces up to N^{4}LO$^+$ [83], which in the three-nucleon cases were augmented by the N^{2}LO three-nucleon potentials. Our calculations have thus rather a "hybrid" character, since the chiral expansion of the nuclear potentials ignores the appearance of the intermediate momentum scale $\sim\sqrt{M_\pi M}$ relevant for the pion absorption processes. Despite this fact our calculations bring important results which should be confronted with predictions achieved within a more consistent framework and with experimental data in the future. In particular our results emphasize the decisive role of the two-nucleon absorption mechanisms in all the studied processes.

TABLE VIII. Absorption rate Γ_{nnn} compared to the result $\Gamma_{^3\mathrm{H}}^{closure}$, obtained using the closure method described in Ref. [82] for negative pion absorption in ^{3}H calculated with the chiral semilocal momentum-space regularized two-nucleon potentials [83] augmented by the consistently regularized three-nucleon force at N^{2}LO [84]. The initial and final states are computed with the two- and three-nucleon forces and the complete transition operator is employed [Full–(SN+2N)–(2NF+3NF)].

	Absorption rates in 10^{15} s^{-1}	
Λ (MeV)	Γ_{nnn}	$\Gamma_{^3\mathrm{H}}^{closure}$
400	1.375	1.373
450	1.110	1.109
500	1.002	1.001
550	1.061	1.059

Final state interactions effects are also important. Not only do they reduce the values of the total absorption rates but they alter the shapes of the differential rates. On the other hand, three-nucleon force effects are relatively small.

Our LO-MCS result for the rate of the $\pi^- + {}^2\mathrm{H} \to n + n$ process evaluated for the N^{4}LO$^+$ wave functions is $\Gamma_{nn} = (1.3^{+0.2}_{-0.1} \pm 1.0) \times 10^{15}$ s^{-1}, where the central value and the first (asymmetric) uncertainty correspond to the average and the spread of the results obtained for four different cutoffs, respectively, while the second error is related to the LO-MCS truncation uncertainty estimated very conservatively. The predicted values for Γ_{nn} show very good agreement with the experimental data from the hadronic ground-state broadening in pionic deuterium [90,91] as well as with the previous EFT calculations [41,44]. Using the same chiral NN interactions and pion transition operators we predict the pion capture rates on ^{3}He and ^{3}H; see Eqs. (4.10)–(4.12) and (4.19). While the central values of the predicted capture rates on ^{3}He are found to be systematically smaller than the experimental data, our LO-MCS results are consistent with the data within error bars. The comparison of our normalized predictions for Γ_{pnn} with the experimental data from Ref. [65], where relative contributions to the total rate Γ_{pnn} from four regions in the phase-space were reported, reveals a rough agreement with the data.

Our predictions for the total absorption rates depend on the order of the two-nucleon potential and on the value of the cutoff parameter Λ used to construct the NN wave functions. The cutoff dependence could be expected since only LO-MCS absorption operators are employed in the present calculations. However, even if the softest cutoff ($\Lambda = 400$ MeV) is included, which might already cut some part of the intermediate range physics relevant for pion absorption, the spread in the results caused by the cutoff variation is much weaker than the LO-MCS truncation error. It would therefore be important to improve the calculations by including the production operators up to and including N^{2}LO-MCS, where two unknown $NN \to NN\pi$ contact interactions start to contribute. Once these contact terms are fixed to low-energy data in $p + p \to {}^2\mathrm{H} + \pi^-$ and $p + p \to p + p + \pi^0$, respectively, the cutoff dependence of the predicted pion absorption rates on ^{3}He and ^{3}H is expected to be reduced also. Such a study would therefore test the field-theoretical consistency of the proposed EFT framework. It would also allow to reduce the truncation error of the results for the rates based on the MCS expansion roughly by a factor of 6 and thus provide an important test of our understanding of pion production in few-nucleon systems.

We definitely think that the above mentioned processes are worth further theoretical and experimental studies, since they could bring interesting insights into neutron-neutron and three-neutron interactions. Also the corresponding pion absorption on ^{4}He, where some experimental data are available [97], is very interesting because of three different reaction channels.

ACKNOWLEDGMENTS

This work was supported in part by BMBF (Grant No. 05P21PCFP4), by DFG and NSFC through funds provided

to the Sino-German CRC 110 "Symmetries and the Emergence of Structure in QCD" (NSFC Grant No. 12070131001, Project ID 196253076-TRR 110), and by ERC Nuclear Theory (Grant No. 885150). One of the authors (J.G.) gratefully acknowledges the financial support of the JSPS International Fellowships for Research in Japan (ID S19149). The numerical calculations were partly performed on the supercomputers of the JSC, Jülich, Germany.

[1] O. V. Maxwell, W. Weise, and M. Brack, Nucl. Phys. A **348**, 388 (1980).
[2] W. Grein, A. König, P. Kroll, M. P. Locher, and A. Švarc, Ann. Phys. (NY) **153**, 301 (1984).
[3] J. Vogelzang, B. L. G. Bakker, and H. J. Boersma, Nucl. Phys. A **452**, 644 (1985).
[4] T. Mizutani and D. S. Koltun, Ann. Phys. (NY) **109**, 1 (1977).
[5] Y. Avishai and T. Mizutani, Nucl. Phys. A **326**, 352 (1979).
[6] D. S. Koltun and T. Mizutani, Phys. Rev. C **22**, 1657 (1980).
[7] Y. Avishai and T. Mizutani, Nucl. Phys. A **338**, 377 (1980).
[8] Y. Avishai and T. Mizutani, Nucl. Phys. A **352**, 399 (1981).
[9] M. Betz and T.-S. H. Lee, Phys. Rev. C **23**, 375 (1981).
[10] B. Blankleider and I. R. Afnan, Phys. Rev. C **24**, 1572 (1981).
[11] Y. Avishai and T. Mizutani, Phys. Rev. C **27**, 312 (1983).
[12] A. S. Rinat and Y. Starkand, Nucl. Phys. A **397**, 381 (1983).
[13] H. Garcilazo and T. Mizutani, Few-Body Syst. **5**, 127 (1988).
[14] Y. Avishai and T. Mizutani, J. Phys. G **6**, L203 (1980).
[15] Y. Avishai and T. Mizutani, Nucl. Phys. A **393**, 429 (1982).
[16] D. Ashery and J. P. Schiffer, Ann. Rev. Nucl. Part. Sci. **36**, 207 (1986).
[17] H. J. Weyer, Phys. Rep. **195**, 295 (1990).
[18] *Mesons in Nuclei*, edited by M. Rho and D. Wilkinson (North-Holland, Amsterdam, 1979).
[19] J. M. Eisenberg and D. S. Koltun, *Mesons and Nuclei: Theory of Meson Interactions with Nuclei* (Wiley-Interscience, New York, 1980).
[20] T. E. O. Ericson and W. Weise, *Pions and Nuclei* (Clarendon, Oxford, 1988).
[21] H. Garcilazo and T. Mizutani, *The πNN System* (World Scientific, Singapore, 1990).
[22] H. O. Meyer, M. A. Ross, R. E. Pollock, A. Berdoz, F. Dohrmann, J. E. Goodwin, M. G. Minty, H. Nann, P. V. Pancella, S. F. Pate *et al.*, Phys. Rev. Lett. **65**, 2846 (1990).
[23] G. A. Miller and P. U. Sauer, Phys. Rev. C **44**, R1725(R) (1991).
[24] D. S. Koltun and A. Reitan, Phys. Rev. **141**, 1413 (1966).
[25] C. Hanhart, Phys. Rep. **397**, 155 (2004).
[26] V. Baru, C. Hanhart, and F. Myhrer, Int. J. Mod. Phys. E **23**, 1430004 (2014).
[27] S. Weinberg, Phys. Lett. B **295**, 114 (1992).
[28] T. D. Cohen, J. L. Friar, G. A. Miller, and U. van Kolck, Phys. Rev. C **53**, 2661 (1996).
[29] B. Y. Park, F. Myhrer, J. R. Morones, T. Meissner, and K. Kubodera, Phys. Rev. C **53**, 1519 (1996).
[30] T. Sato, T. S. H. Lee, F. Myhrer, and K. Kubodera, Phys. Rev. C **56**, 1246 (1997).
[31] C. A. da Rocha, G. A. Miller, and U. van Kolck, Phys. Rev. C **61**, 034613 (2000).
[32] C. Hanhart, J. Haidenbauer, M. Hoffmann, U.-G. Meißner, and J. Speth, Phys. Lett. B **424**, 8 (1998).
[33] V. Dmitrašinović, K. Kubodera, F. Myhrer, and T. Sato, Phys. Lett. B **465**, 43 (1999).
[34] S. I. Ando, T. S. Park, and D. P. Min, Phys. Lett. B **509**, 253 (2001).
[35] V. Bernard, N. Kaiser, and U. G. Meissner, Eur. Phys. J. A **4**, 259 (1999).
[36] C. Hanhart, U. van Kolck, and G. A. Miller, Phys. Rev. Lett. **85**, 2905 (2000).
[37] C. Hanhart and N. Kaiser, Phys. Rev. C **66**, 054005 (2002).
[38] E. Epelbaum, H.-W. Hammer, and Ulf-G. Meißner, Rev. Mod. Phys. **81**, 1773 (2009).
[39] R. Machleidt and D. R. Entem, Phys. Rep. **503**, 1 (2011).
[40] E. Epelbaum, H. Krebs, and P. Reinert, Front. Phys. **8**, 98 (2020).
[41] V. Lensky, V. Baru, J. Haidenbauer, C. Hanhart, A. E. Kudryavtsev, and U.-G. Meißner, Eur. Phys. J. A **27**, 37 (2006).
[42] A. A. Filin, V. Baru, E. Epelbaum, H. Krebs, C. Hanhart, A. E. Kudryavtsev, and F. Myhrer, Phys. Rev. C **85**, 054001 (2012).
[43] A. A. Filin, V. Baru, E. Epelbaum, H. Krebs, C. Hanhart, and F. Myhrer, Phys. Rev. C **88**, 064003 (2013).
[44] V. Baru, E. Epelbaum, A. A. Filin, C. Hanhart, H. Krebs, and F. Myhrer, Eur. Phys. J. A **52**, 146 (2016).
[45] E. Epelbaum, A. Nogga, W. Glöckle, H. Kamada, Ulf-G. Meißner, and H. Witała, Phys. Rev. C **66**, 064001 (2002).
[46] T. S. Park, L. E. Marcucci, R. Schiavilla, M. Viviani, A. Kievsky, S. Rosati, K. Kubodera, D. P. Min, and M. Rho, Phys. Rev. C **67**, 055206 (2003).
[47] D. Gazit, S. Quaglioni, and P. Navratil, Phys. Rev. Lett. **103**, 102502 (2009); **122**, 029901(E) (2019).
[48] A. Gardestig and D. R. Phillips, Phys. Rev. Lett. **96**, 232301 (2006).
[49] H. Krebs, E. Epelbaum, and U.-G. Meißner, Ann. Phys. (NY) **378**, 317 (2017).
[50] V. Lensky, V. Baru, J. Haidenbauer, C. Hanhart, A. E. Kudryavtsev, and U.-G. Meißner, Eur. Phys. J. A **26**, 107 (2005).
[51] V. Lensky, V. Baru, E. Epelbaum, C. Hanhart, J. Haidenbauer, A. E. Kudryavtsev, and U. G. Meissner, Eur. Phys. J. A **33**, 339 (2007).
[52] A. K. Opper, E. Korkmaz, D. A. Hutcheon, R. Abegg, C. A. Davis, R. W. Finlay, P. W. Green, L. G. Greeniaus, D. V. Jordan, J. A. Niskanen, G. V. O'Rielly, T. A. Porcelli, S. D. Reitzner, P. L. Walden, and S. Yen, Phys. Rev. Lett. **91**, 212302 (2003).
[53] U. van Kolck, J. A. Niskanen, and G. A. Miller, Phys. Lett. B **493**, 65 (2000).
[54] A. Filin, V. Baru, E. Epelbaum, J. Haidenbauer, C. Hanhart, A. E. Kudryavtsev, and U.-G. Meißner, Phys. Lett. B **681**, 423 (2009).
[55] D. R. Bolton and G. A. Miller, Phys. Rev. C **81**, 014001 (2010).
[56] P. Adlarson *et al.* (WASA-at-COSY Collaboration), Phys. Lett. B **739**, 44 (2014).
[57] P. Adlarson *et al.* (WASA-at-COSY Collaboration), Phys. Lett. B **781**, 645 (2018).
[58] A. Nogga, A. C. Fonseca, A. Gardestig, C. Hanhart, C. J. Horowitz, G. A. Miller, J. A. Niskanen, and U. van Kolck, Phys. Lett. B **639**, 465 (2006).

[59] J. M. Cameron, L. G. Greeniaus, D. A. Hutcheon, C. A. Miller, G. A. Moss, R. P. Liljestrand, H. Wilson, R. Abegg, W. T. H. Van Oers, A. W. Stetz *et al.*, Phys. Lett. B **103**, 317 (1981).
[60] R. Bilger, W. Brodowski, H. Calen, H. Clement, C. Ekstrom, G. Faldt, K. Fransson, L. Gustafsson, B. Hoistad, A. Johansson *et al.*, Phys. Rev. C **65**, 044608 (2002).
[61] S. Dymov, V. Shmakova, D. Mchedlishvili, T. Azaryan, S. Barsov, A. Dzyuba, R. Engels, R. Gebel, P. Goslawski, B. Gou *et al.*, Phys. Lett. B **762**, 102 (2016).
[62] I. Schwanner, G. Backenstoss, W. Kowald, L. Tauscher, H. J. Weyer, D. Gotta, and H. Ullrich, Nucl. Phys. A **412**, 253 (1984).
[63] O. A. Zaimidoroga, M. M. Kulyukin, R. M. Sulyaev, I. V. Falomkin, A. I. Filippov, V. M. Tsupko-Sitnikov, and Yu. A. Shcherbakov, J. Exptl. Theoret. Phys. (U.S.S.R.) **51**, 1646 (1966) [Sov. Phys. JETP **24**, 1111 (1967)].
[64] J. McCarthy, T. Meyer, R. C. Minehart, E. A. Wadlinger, K. O. H. Ziock, and J. Vincent, Phys. Rev. C **11**, 266 (1975).
[65] D. Gotta, M. Dörr, W. Fetscher, G. Schmidt, H. Ullrich, G. Backenstoss, M. Izycki, W. Kowald, I. Schwanner, P. Weber, and H. J. Weyer, Phys. Rev. C **51**, 469 (1995).
[66] S. Schneider, J. Haidenbauer, C. Hanhart, and J. A. Niskanen, Phys. Rev. C **67**, 044003 (2003).
[67] L. Canton and L. G. Levchuk, Phys. Rev. C **71**, 041001(R) (2005).
[68] V. Lensky, V. Baru, J. Haidenbauer, C. Hanhart, A. E. Kudryavtsev, and U.-G. Meißner, Phys. Lett. B **648**, 46 (2007).
[69] V. Baru, C. Hanhart, M. Hoferichter, B. Kubis, A. Nogga, and D. R. Phillips, Nucl. Phys. A **872**, 69 (2011).
[70] V. Baru, C. Hanhart, M. Hoferichter, B. Kubis, A. Nogga, and D. R. Phillips, Phys. Lett. B **694**, 473 (2011).
[71] V. Baru, J. Haidenbauer, C. Hanhart, and J. A. Niskanen, Eur. Phys. J. A **16**, 437 (2003).
[72] S. Liebig, V. Baru, F. Ballout, C. Hanhart, and A. Nogga, Eur. Phys. J. A **47**, 69 (2011).
[73] W. Glöckle, H. Witała, D. Hüber, H. Kamada, and J. Golak, Phys. Rep. **274**, 107 (1996).
[74] J. Golak, R. Skibiński, H. Witała, W. Glöckle, A. Nogga, and H. Kamada, Phys. Rep. **415**, 89 (2005).
[75] R. Skibiński, J. Golak, H. Witała, W. Glöckle, and A. Nogga, Eur. Phys. J. A **24**, 31 (2005).
[76] J. Golak, R. Skibiński, H. Witała, K. Topolnicki, A. E. Elmeshneb, H. Kamada, A. Nogga, and L. E. Marcucci, Phys. Rev. C **90**, 024001 (2014).
[77] J. Golak, R. Skibiński, H. Witała, K. Topolnicki, H. Kamada, A. Nogga, and L. E. Marcucci, Phys. Rev. C **94**, 034002 (2016).
[78] R. Skibiński, J. Golak, K. Topolnicki, H. Witała, E. Epelbaum, H. Krebs, H. Kamada, Ulf-G. Meißner, and A. Nogga, Phys. Rev. C **93**, 064002 (2016).
[79] V. Urbanevych, R. Skibiński, H. Witała, J. Golak, K. Topolnicki, A. Grassi, E. Epelbaum, and H. Krebs, Phys. Rev. C **103**, 024003 (2021).
[80] J. Golak, R. Skibiński, K. Topolnicki, H. Witała, A. Grassi, H. Kamada, and L. E. Marcucci, Phys. Rev. C **98**, 015501 (2018).
[81] J. Golak, R. Skibiński, K. Topolnicki, H. Witała, A. Grassi, H. Kamada, and L. E. Marcucci, Phys. Rev. C **100**, 064003 (2019).
[82] J. Golak, R. Skibiński, K. Topolnicki, H. Witała, A. Grassi, H. Kamada, A. Nogga, and L. E. Marcucci, Phys. Rev. C **98**, 054001 (2018).
[83] P. Reinert, H. Krebs, and E. Epelbaum, Eur. Phys. J. A **54**, 86 (2018).
[84] P. Maris, E. Epelbaum, R. J. Furnstahl, J. Golak, K. Hebeler, T. Hüther, H. Kamada, H. Krebs, Ulf-G. Meißner, J. A. Melendez, A. Nogga, P. Reinert, R. Roth, R. Skibiński, V. Soloviov, K. Topolnicki, J. P. Vary, Yu. Volkotrub, H. Witała, and T. Wolfgruber (LENPIC Collaboration), Phys. Rev. C **103**, 054001 (2021).
[85] V. Bernard, N. Kaiser, and U.-G. Meißner, Int. J. Mod. Phys. E **4**, 193 (1995).
[86] J. Golak, D. Rozpędzik, R. Skibiński, K. Topolnicki, H. Witała, W. Glöckle, A. Nogga, E. Epelbaum, H. Kamada, Ch. Elster, and I. Fachruddin, Eur. Phys. J. A **43**, 241 (2010).
[87] R. Skibiński, J. Golak, K. Topolnicki, H. Witała, H. Kamada, W. Glöckle, and A. Nogga, Eur. Phys. J. A **47**, 48 (2011).
[88] W. Glöckle, *The Quantum Mechanical Few-Body Problem* (Springer-Verlag, Berlin, 1983).
[89] J. D. Bjorken and S. D. Drell, *Relativistic Quantum Mechanics* (McGraw-Hill, New York, 1998).
[90] T. Strauch, F. D. Amaro, D. Anagnostopoulos, P. Buhler, D. S. Covita, H. Gorke, D. Gotta, A. Gruber, A. Hirtl, P. Indelicato *et al.*, Eur. Phys. J. A **47**, 88 (2011).
[91] T. Strauch, F. D. Amaro, D. F. Anagnostopoulos, P. Buhler, D. S. Covita, H. Gorke, D. Gotta, A. Gruber, A. Hirtl, P. Indelicato *et al.*, Phys. Rev. Lett. **104**, 142503 (2010).
[92] J. A. Niskanen, Phys. Rev. C **43**, 36 (1991).
[93] L. L. Kiang, T.-S. H. Lee, and D. O. Riska, Phys. Rev. C **50**, 2703 (1994).
[94] L. E. Marcucci, M. Piarulli, M. Viviani, L. Girlanda, A. Kievsky, S. Rosati, and R. Schiavilla, Phys. Rev. C **83**, 014002 (2011).
[95] G. R. Mason, G. A. Beer, M. S. Dixit, S. K. Kim, J. A. Macdonald, A. Olin, R. M. Pearce, W. C. Sperry, and J. S. Vincent, Nucl. Phys. A **340**, 240 (1980).
[96] P. Truoel, H. W. Baer, J. A. Bistirlich, K. M. Crowe, N. de Botton, and J. A. Helland, Phys. Rev. Lett. **32**, 1268 (1974).
[97] E. Daum, S. Vinzelberg, D. Gotta, H. Ullrich, G. Backenstoss, P. Weber, H. J. Weyer, M. Furic, and T. Petković, Nucl. Phys. A **589**, 553 (1995).